Informes Técnicos Ciemat

1328

Septiembre, 2014

GIS-Based Method to Evaluate the Photovoltaic Potential in the Urban Environments: The Particular Case of Miraflores de la Sierra

A. Verso

GOBIERNO DE ESPAÑA

MINISTERIO DE ECONOMÍA Y COMPETITIVIDAD

Ciemat

Centro de Investigaciones Energéticas, Medioambientales y Tecnológicas

Informes Técnicos Ciemat

1328

Septiembre, 2014

GIS-Based Method to Evaluate the Photovoltaic Potential in the Urban Environments: The Particular Case of Miraflores de la Sierra

A. Verso

J. Domínguez [1]

J. Amador [1]

1 Dirección

Departamento de Energía

Toda correspondencia en relación con este trabajo debe dirigirse al Servicio de Información y Documentación, Centro de Investigaciones Energéticas, Medioambientales y Tecnológicas, Ciudad Universitaria, 28040-MADRID, ESPAÑA.

Las solicitudes de ejemplares deben dirigirse a este mismo Servicio.

Los descriptores se han seleccionado del Thesauro del DOE para describir las materias que contiene este informe con vistas a su recuperación. La catalogación se ha hecho utilizando el documento DOE/TIC-4602 (Rev. 1) Descriptive Cataloguing On-Line, y la clasificación de acuerdo con el documento DOE/TIC.4584-R7 Subject Categories and Scope publicados por el Office of Scientific and Technical Information del Departamento de Energía de los Estados Unidos.

Catálogo general de publicaciones oficiales
http://www.060.es

Depósito Legal: M-26385-2011
ISSN: 1135-9420
NIPO: 721-14-041-7

Editorial CIEMAT

CLASIFICACIÓN DOE Y DESCRIPTORES

S14
SOLAR ENERGY; SOLAR RADIATION; GEOGRAPHIC INFORMATION SYSTEMS;
PHOTOVOLTAIC CONVERSION; URBAN AREAS; ROOFS; SPAIN

GIS-Based Method to Evaluate the Photovoltaic Potential in the Urban Environments: The Particular Case of Miraflores de la Sierra

Verso, A.

89 pp. 41 ref. 55 figs. 8 tables

Abstract:

The objective of this work is to develop a model based on geographic information system (GIS), Light Detection and Ranging (LIDAR) and hourly horizontal radiation data to explore the possibility to install Photovoltaic (PV) systems in urban environments and to evaluate the annual production of electricity. The new model is tested on a small area of the municipality of Miraflores de la Sierra.

The LIDAR data allow an accurate description of the urban environments trough the creation of a digital surface model. This is used to calculated the shadow of the different elements and to calculate the local inclination and orientation of the roofs. Two typologies of roofs are differentiated. The first one where the PV panels are placed parallel to the roof and the second one where the panels are disposed at the optimum using structures. The radiation incident on the panels is calculated with a geometric method starting from the hourly horizontal radiation decomposed in his diffuse and direct components. Finally, the effective production is evaluated taking into account the efficiency of the panels and different losses especially the ones due to temperature. The five most common panel's technologies are considered

.

Estimación del Potencial Fotovoltaico en un Entorno Urbano Mediante SIG. Caso de Estudio: Miraflores de la Sierra

Verso, A.

89 pp. 41 ref. 55 figs. 8 tablas

Resumen:

El objetivo de este trabajo es desarrollar un modelo basado en sistema de información geográfica (SIG), datos Light Detection and Ranging (LIDAR) y datos de radiación horaría sobre superfice horizontal para explorar la posibilidad de instalar sistemas fotovoltaicos (PV) en los entornos urbanos y para evaluar la producción anual de electricidad. Se ha probado el nuevo modelo en una pequeña área del municipio de Miraflores de la Sierra.

Los datos LIDAR permite una descripción precisa de los entornos urbanos a través de la creación de un modelo digital de superficie. Esto se utiliza para calcular la sombra de los diferentes elementos y para conozer la orientación y la inclinación locales de los tejados. Esta información permite dividir los tejados en dos tipologías: los tejados inclinados donde los paneles están montados paralelos al tejado y tejados planos o casi planos, donde los paneles se colocan a la orientación y la inclinación deseada. La radiación incidente sobre los paneles se calcula con un método geométrico a partir de la radiación horaría sobre superfice horizontal descompuesta en su componentes difusa y directa. Por último, la producción efectiva se evalúa teniendo en cuenta la eficiencia de los paneles y la difretentes pérdidas especialmente las debidas a la temperatura. Se consideran las cinco tecnologías mas común de paneles.

.

.

Contents

List of Figures

Introduction

Currently half the world's population lives in urban areas and according to the UN projections is estimated to reach up to 60% in two decades[1]. As reflected in Directive 2010/31/UE, 40% of total energy consumption in the EU is for the buildings. These conditions have led the EU to promote a program to develop the energy efficiency in buildings and the integration of renewable energies. In the 2020 new buildings or renovated ones will have to fulfill high requirements of energy efficiency, and part of the energy consumption should come from renewable sources. Amongst the different options solar energy has an important role to play [1]. Photovoltaic (PV) systems have the advantage to generate energy in the same place where it is consumed and that are easy to integrate in the urban environment. To implement policies focused on improve the PV generation it is important to determine what percentage of the energy's needs of cities can be covered by own production of electricity. In this sense, maps of photovoltaic potential on the urban/regional scales are fundamental and as well these can increase the environmental awareness of residents and improve the sustainable image of a city [2]. The energy resources depends on the characteristics of the area as geographical location and climatic conditions therefore, geographic information system (GIS) is a perfect tool for this analysis

In last few years has been developed models capable to evaluate the solar potential and to predict the energy production in different spatial and temporal scales [3, 4, 5]. For example Izquierdo [6] developed an integrated methodology in which estimate the surface of roofs available for solar systems in buildings, in this case the study area includes all Spain, and is based on the municipality as unity.

The main problems are the assessment of the solar radiation and the evaluation of the useful surface. The most simple approximation of the solar potential is a constant assumption whereby every point on a rooftop receives

[1]State of the World's Cities 2008/2009 Harmonious Cities. ONU Habitat

the same amount of solar irradiation. Usually this value is derived from annual global horizontal irradiation measurements from a nearby weather station. In this case the irradiation is independent from orientation and surrounding context and it will be inaccurate in many cases, for example buildings with peaked roofs where each surface of the roof has a different orientation. Usually the influence of the orientation and the inclination are just weight with some factor obtained from the statistic of the shape of the buildings. In a similar statistic way is treated the local urban context such as trees and neighboring buildings, which shade building rooftops [7, 8]. In some case orthophotographic image analysis techniques are used [9]. A more detailed calculation is provide by the National Renewable Energy Laboratory with the PVWatts web service [2] in which hourly solar irradiation distributed on a 40 km square grid for the entire United States is calculated[10]. This toolbox calculate the energy production starting from the hourly data of a the typical meteorological year and taking into account the PV panel inclination, orientation and temperature and as well a climate-based sky models. The accuracy is high and was showed in [11] that the discrepancy between the value obtained with this method and real measured value is around 10%. The disadvantage of this approach is that the environment with his shadow and reflection property is not considered. Moreover it is complicate to automatize the calculation for large area where the inclination and orientation of each point must be input separately. A similar service is provided by PVGIS [3] that allows to calculate irradiation map for Europe and Africa and has well to calculate PV production. A different approach is used by the Esri's Solar Analyst plugin [12] this calculatse the irradiation from the sun's position and the a 3D model of the area, this allows to take into account automatically the real slop of the roof surface and an accurate description of the different elements in the urban context and their shadows. The drawback is that it does not take into account local conditions of the atmosphere and his variation during the year. In Solar Analyst, the ratio between direct and diffuse radiation and sky transmissivity are constant values throughout the year. This lead to big inaccuracy on the calculation of the year energy production [13]. The r.sum solve in part this problem considering the variation of the sky transmissivity and the ratio between direct and diffuse radiation[14]. This toolbox allows as well spatial change of these values, for this reason is suitable to analyze large area whit different climate zones. Other alternatives have been proposed by [15], [3] and [16]. In [15] Solar Analyst is used but

[2] www.nrel.gov/rredc/pvwatts/

[3] PVGIS (Photovoltaic Geographical Information System) is a database of radiation calculated from satellite data developed by the Institute for Energy and Transport pf the European Commission (http://re.jrc.ec.europa.eu/pvgis/apps4/pvest.phpadra).

on a monthly bases so some variation on the atmosphere are included in the model. This approach reduces the model monthly radiation variation with respect to the PVGIS database from about 20% to less than 2% [17]. In [3] a Daysim backward-raytracing daylight simulation engine was developed, this allow an accurate description of the different buildings surface and there reflection. The base of all these new models is an accurate description of the urban area and this is obtained from Light Detection and Ranging (LIDAR) data [18, 19, 20] that allow to know the height of all the element of the area. The common resolution is about 1m but the technology is moving fast to higher resolution. This work tries to move in this direction building an alternative approach to the problem of the irradiation and as well developing a new method to calculate the useful roof area for PV panels that allows to take in to account special type of roof as the flat one.

There are software (as PVsyst) that allow a really detailed evaluation of a PV system, these software calculate the irradiation on the PV panels and his energy production. The quality of the prediction of this kind of software is relay high but the scope it is different from the systems based on GIS, this are used to simulate at the level of final project single system however they can be large and complex, on the other hand GIS based methods can evaluate entire city or country and they can help giving information before to start a project.

Chapter 1

The Model

The objective of this work is to develop a GIS-based model to explore the possibility to install solar systems for electric generation in urban environments and to evaluate the annual production of electricity. This work is based on the model developed in [13], the goal was improve it. Major progress have been made in three directions: first the evaluation of the photovoltaic potential, second the utilization of flat roofs and third the analysis of the losses in particular the ones due to inclination, orientation, shadow and temperature. In the Fig.(1.1) it is possible to see the basic diagram of our model. The model requires two kind of information, about the location, in this case a portion of the city of Miraflores de la Selva (Madrid, Spain) and about the solar resource (horizontal irradiation and sun's position). The model is able to process this information and automatically assessment the PV potential of the roofs. The first step is create a three dimensional model of the urban environment in order to know the position and the shape of the buildings and at the same time to individuate the presence of obstacles that can whit their the shadow disturb the PV panels. At this point it is fundamental the quality of the data used for the 3D model [21]. In this work LIDAR data with spatial resolution of approximately $1m^2$ are used (as done in [13]). This data are suitable to recognize the roofs and others objects as trees but unfortunately the resolution is not high enough to detect small objects or parts of the buildings as chimney and air-conditioning systems that can be present on the roofs and can affect the operation of the PV system. But probably in short time data with a higher resolution will be available and the model was built in order to be able to work regardless of the resolution. The second step is determinate in first approximation the areas suitable for the PV panels.

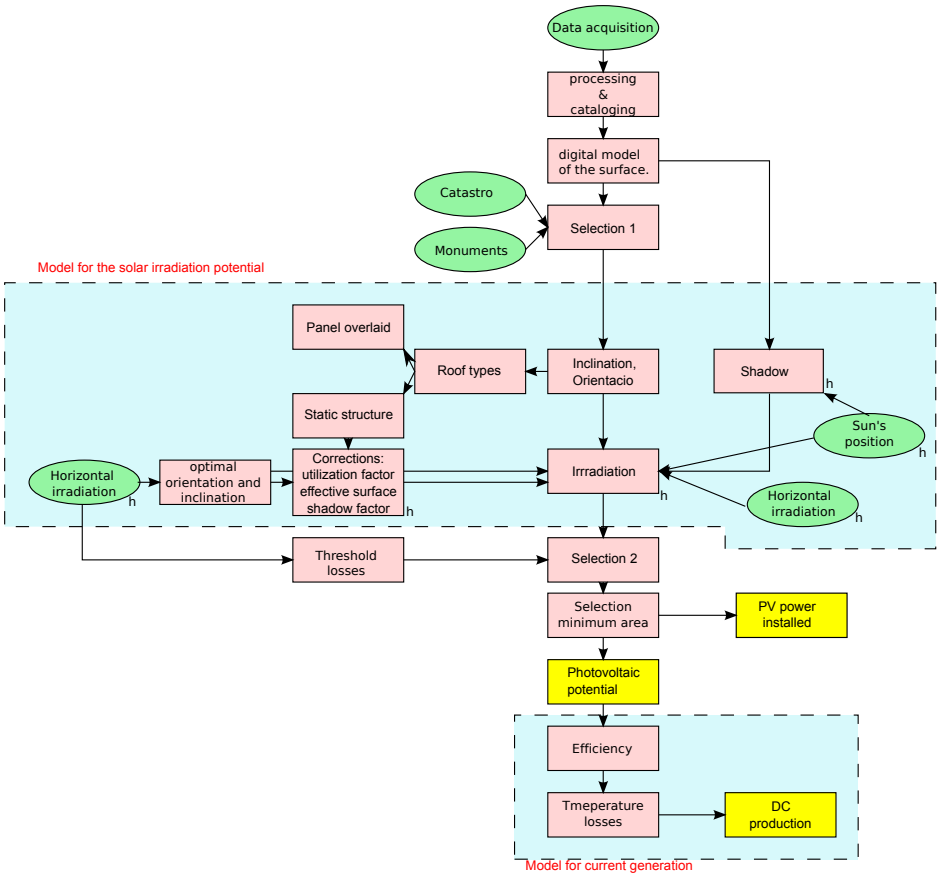

Figure 1.1: Model

After a map with the orientations and inclination of each point of the roofs is created. This information allows to divide the roofs in two typologies. Sloping roofs where the panels are mounted with some simple structures parallel to the roof and flat or almost flat roofs where the panels are mounted on more complex structures that allow to arrange the panels with the orientation and inclination desired. This is an important improvement of the model because in the realty is a common practice to use structures to optimize the disposition of solar panels. This flexibility in the positioning of the panels substantially changes the amount of electricity produced. There are different manner to optimize the disposition of the panels. In this work the best inclination and orientation are determined looking for the maximum annual production per square meter of panel.

The second improvement was change the method to calculate of the solar irradiation. In [13] the solar irradiation was calculated using "Solar Analysis"

a toolbox included in ArcGis assuming that the panel surface coincides with the one of the roof. This toolbox calculates the irradiation from the sun's position and the 3D mode, so allows an accurate description of the shadows of the different elements. It has significant limitations for calculate annual city-scale photovoltaic potential maps. The first limitation is that it does not take into account local conditions of the atmosphere and his variation during the year. Already in [13] has been noticed how this method underestimate of about a 30% the annual irradiation compared to data obtained with PVGIS and Adrase [1]. Now the irradiation's map is calculated starting from the hourly irradiation on a horizontal surface with a geometric method. In this way it is possible to capture the influence of the change of the atmosphere. Moreover this method allows to calculate the radiation on panels that are not parallel to the roof. The geometric approach developed by Hay and Davis [22, 23] is used together with the shadow generated with the "Hillshade" toolbox from the 3D model.

Summing over a year the hourly irradiation gives an irradiation map and for each point the losses due the orientation, inclination and shadow are calculated respect to the maximum. The losses are calculated without any empirical equation therefore a more reliable result than in [13] is obtained. With these results the locations where the losses are higher and it is not convenient to place PV panels are eliminated. After that, a last filter excludes the areas that are too small for a PV panel.

Afterwards, the effective annual production of energy of AC current is caluculated using the eqaution:

$$E_{annual} = e\, A_{PV} \sum_{h} PR\, I_g^h \tag{1.1}$$

with I_g^h the hourly irradiation on the panel, e the efficiency, A_{PV} the area of the PV panels and PR performance ratio. The temperature losses are analyzed closely and an efficiency depending on the technology and on how the panels are mounted is defined.

[1] Adrase is a web page developed by the CIEMAT in collaboration whit the "Union Española Fotovoltaica". This provide the data of the solar irradiation calculated from satellite's images and measurement done in 50 radiometric stations by the Agencia Estatal de Meteorología (AEMET).(www.adrase.es)

Chapter 2

Data

2.1 Area of study

Miraflores de la Sierra is a municipality located in the region of the Cuenca Alta del Manzanares 49 km north of Madrid.

It has an area of $59,66 km^2$ and is located at latitude $40^o48'41''$N and longitude $3^o46'7''$W. The maximum height of Miraflores de la Sierra is the peak Najarra (2120 m.). The town is surrounded by forest, the Scots pine and oaks are the most representative species in the region. At lower altitudes, where slopes start to decrease, the oak is the dominant species and a grassland environment (used for livestock uses) is present. The urban center is located at 1145 m, south of "Pico de la Pala" and the "Sierra Morcuera". Most of it is built between 1000 and 1200 m with an average terrain inclination of 20.89%.

The climate in Miraflores de la Sierra is characteristic of the interior of Spain and can be classified as continental. The average annual temperature is 10.9ºC and average rainfall are of 686 mm [1]. During the summer the climate is mild with an average maximum temperature of 29.9ºC while in the winter the minimum average temperature is -1.20ºC. Miraflores de la Sierra is largely a residential area but farmers and small industry are present as well in the region

The municipality has 5979 inhabitants (INE, 2012) and a population density of 105.53 inhabitants per km^2. The population increases substantially during the summer months as the town has 65% of second homes. The con-

[1] www.aemet.es/es/serviciosclimaticos/datosclimatologicos.

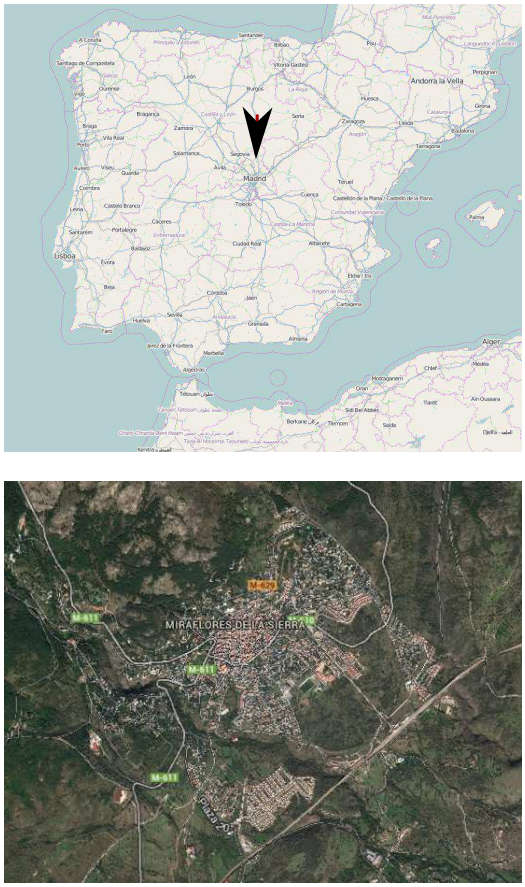

Figure 2.1: Location of the area of study (the figures are from www.openstreetmap.org/ and www.google.es/maps/).

Urban distribution	Land cover (%)	Surface (ha)	Surface (%)
Continuous	> 80	10.66	5.68
Dense discontinuous	$50 - 80$	44.64	23.82
Medium density discontinuous	$30 - 50$	31.60	16.86
Low density	$10 - 30$	38.38	20.47
Very low density	< 10	62.18	33.17

Table 2.1: Urban distribution (Date from the "Urban Atlas" www.eea.europa.eu/data-and-maps/data/urban-atlas).

figuration of the houses is not uniform and as usual in most of the urban centers, the downtown has a high concentration of buildings and a distribution not too homogeneous. Away from the center the urban structure reaches a higher order and lower density. In the complex, the town is characterized by a low density of single family houses usually surrounded by vegetation. The pitched roof with two slopes is the most common but there are also some buildings with more complex roof and buildings with flat roof.

2.2 Land register

The Spanish Land Registry ("Direcciòn General de Catastro") provides a vector map with the information of all buildings and their characteristics in "shapefile" format. From the cadastral parcel (type, shape and cadastral reference), city blocks, buildings delimitation (constructive elements and number of floors), roads, hydrography and roads are obtained.

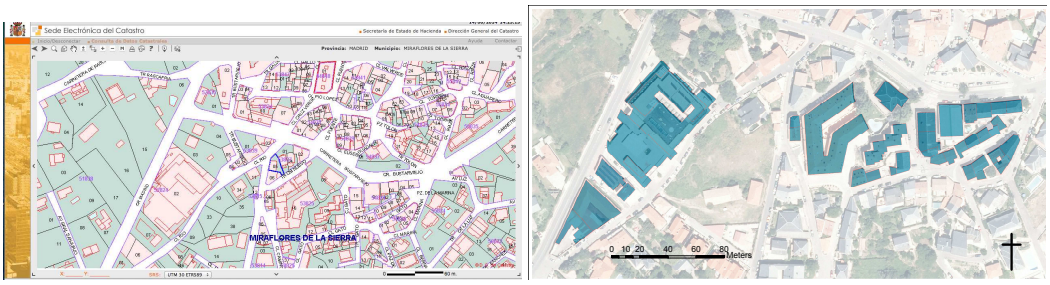

Figure 2.2: At the left, the web page of the "Direcciòn General de Catastro". At the right selection of the buildings included in the study area.

2.3 Monuments and landmark buildings

The Spatial Data Infrastructure Community of Madrid (IDEM)[2] provides data concerning territorial boundaries (cities, urban centers, censarles health areas) and points of interest (public administration, schools, tourism, transport...). Based on the data provided by IDEM and on the tourist map, a

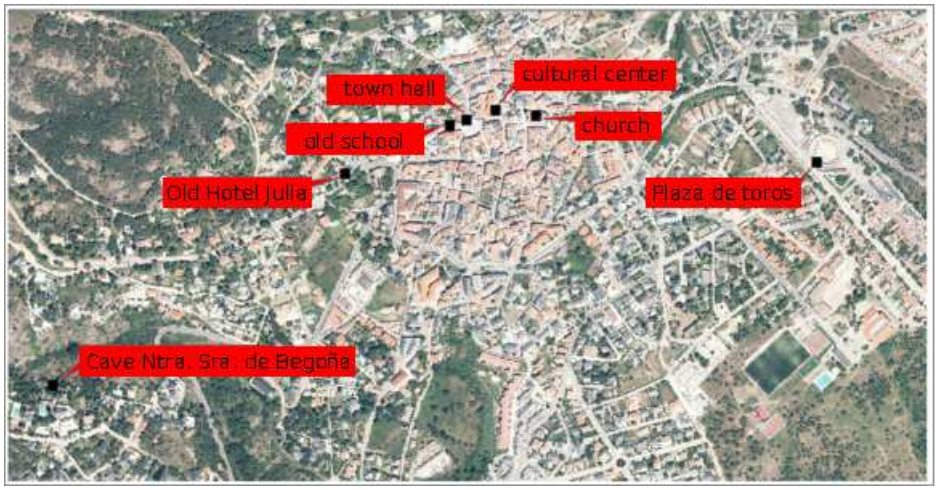

Figure 2.3: Map of the monuments and landmark buildings located in the municipality (Source: IDEM).

point layer is generated with the distribution of all those monuments and buildings located in the municipality that in reason of their unique characteristics are not suitable for the installation of photovoltaic systems.

2.4 Lidar

The LIDAR data constitutes the base to performing the analysis. From this data a digital surface models (DSM) is created. LIDAR is a technology that uses laser light pulses to sample a surface and determinate the height and shape of any element present on the ground such as trees, buildings, infrastructure and vehicles.

The main advantages of LIDAR sensors are the high resolution of the captured data and the ability to obtain information under the cover of veg-

[2]Consejería de Medio Ambiente y Ordenación del Territorio, Comunidad de Madrid, Infraestructura de Datos Espaciales Comunidad de Madrid www.madrid.org/cartografia/idem

etation. Another advantage of LIDAR technology is the capability of the sensor to collect information from several reflection of each laser pulse emitted increasing the quality of the three-dimensional shape of the detected elements. When a laser pulse is emitted can be directly reflected by an object, or can be bounced by different reflective surfaces until it reaches the ground. When only a reflection is collected usually represents the ground, and several reflections correspond to elements with different heights such as trees and buildings. LIDAR measurements done from air are used. In this case the air transport may be a plane or a helicopter. Such system is equipped with a laser scanning system to determine the distance of the elements, measuring the time between the light beam emission and the detection of the reflected signal and a GPS (Global Positioning System) to know the position of the detection system itself. It is also necessary an INS (Inertial Navigation System) to determinate the orientation and inclination of the plane.

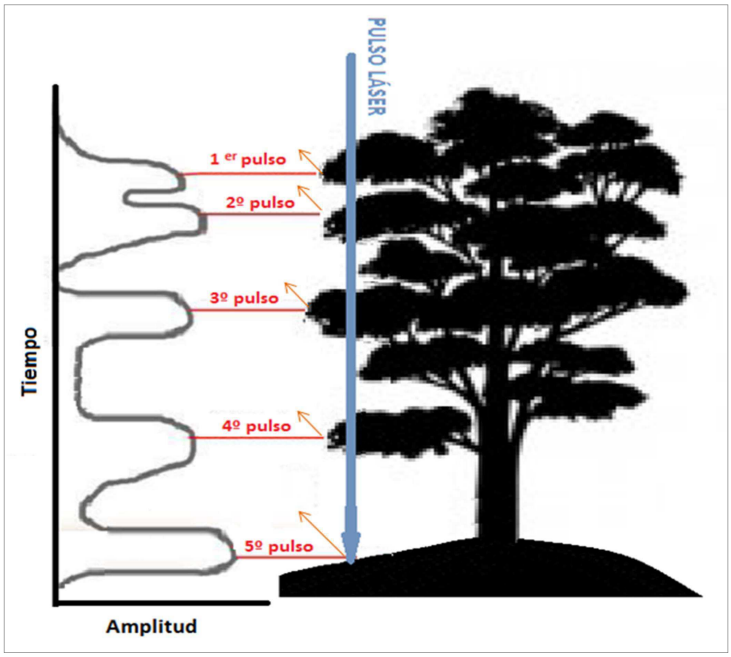

Figure 2.4: Scheme of detection of vegetation with lase pulse (Figure adapted from [13]).

Using the position of the laser sensor and his measurements a georeferenced point cloud of elevation is obtained with high accuracy. Usually the data are saved in LAS format developed by the American Society for Photogrammetry & Remote Sensing (ASPRS). Subsequently the LIDAR points are filtered and classified assigning a corresponding numerical value repre-

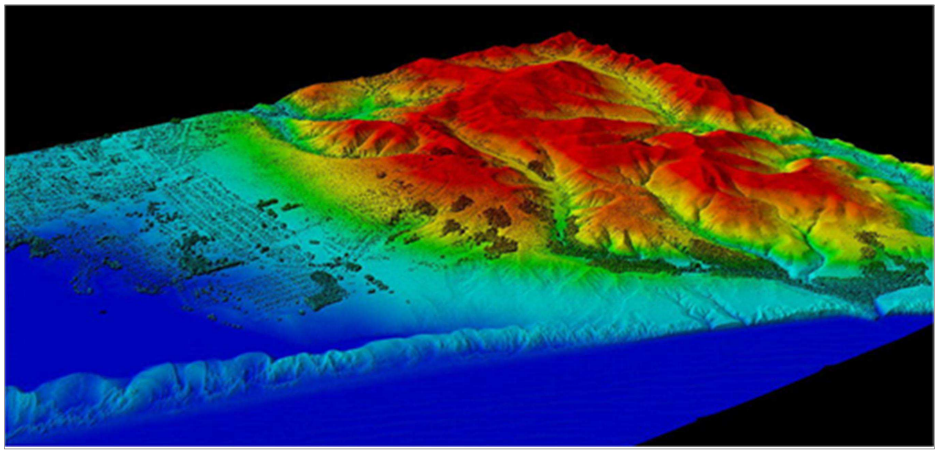

Figure 2.5: LIDAR's cloud points

senting the object that has reflected the laser pulse. It is possible to assign different types of classifications which may include the categories of soil/terrain and vegetation cover. LIDAR's data of the flight of National Plan of Aerial Orthophotography (PNOA) provided by the (IGN) National Geographic Institute are used. The data have the following characteristics:

- Flight date: Year 2010.
- Geodesic reference System ETRS89 and Designing Cartografica UTM zone 30.
- The files are in in the format "las", version 1.2, and each covers an area of $2x2$ km with an average density of 0.5 points/m^2 so, the spacing between points is smaller than 1.41 m.
- The files are classified automatically including vegetation and buildings according to the standards established by the ASPRS.
- The points have color information (RGB) from the orthophotography.

2.5 Solar radiation

The knowledge of the solar radiation at a given site is crucial for estimate the electricity produced by a photovoltaic systems. The best option is to have a direct hourly ground measurement during several years but this rarely the

case. A viable option is to derive the solar radiation from satellite data [24]-[25]combined with various meteorological data. Geostationary satellites provides information of the earth's atmosphere and clouds with high spatial and temporal resolution. In particular the result obtained in [26] with a new statistical method [27]-[28] are used. This works are based on data of Meteosat of a time period from January 1994 to December 2004, with a spatial resolution of 2.5 km × 2.5 km at nadir and a temporal resolution of 30 min.

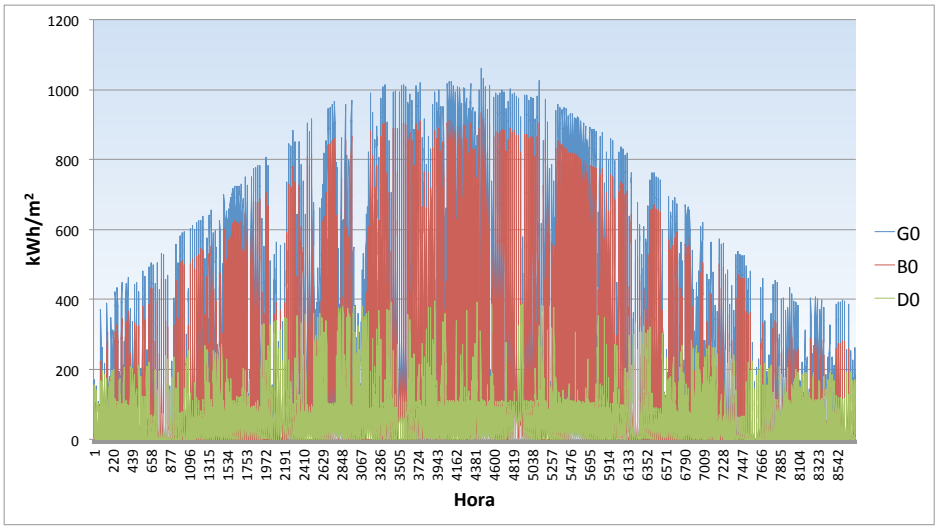

Figure 2.6: Evolution during a year of the total radiation on a horizontal surface $G0$ in his components: the direct radiation $B0$ and the diffuse one $D0$ (figur2 obtained with the date of [28]).

This provides us a serie of the global hourly solar irradiance on a horizontal surface and of the direct normal irradiance. This data have a relative mean bias error of 0.32% [28]. For a small region is appropriate to neglect any spatial dependence of the radiation. In the Ch.4 it will explained in detailes how to calculate from this data a radiation map for the area of study.

Chapter 3

Preparation of the data

The model has been tested on a small but representative area of study. In this region there are some typical family houses with sloping roofs and two building with flat roofs, a hotel and a petrol station.

Figure 3.1: Area of study.

3.1 Digital surface model

In order to calculate a detailed map of the solar potential a 3 dimensional model of the area of interest is created taking into account all the elements

(surface terrain, buildings, trees...). This is done starting from the LIDAR's data (see Sec.2.4).

3.1.1 Classification and processing of the LIDARS's data

The LIDAR's point cloud presents a preliminary automatic classification but not all elements are properly classified. For example part of the roofs of buildings is defined as high vegetation areas. For this reason, it is necessary a reclassification of the LIDAR data to define more precisely as possible the delimitation of the different elements. The "VRMesh V7.6 Studio" program allows to automatically classify point clouds and also to make manual changes in those areas where the classification has not been precise enough. It is a multy-steps process. First the software does an automatic classification of the data using three categories: vegetation, building and ground. For any of these categories it is possible to fix the value of some parameters to have an accurate classification.

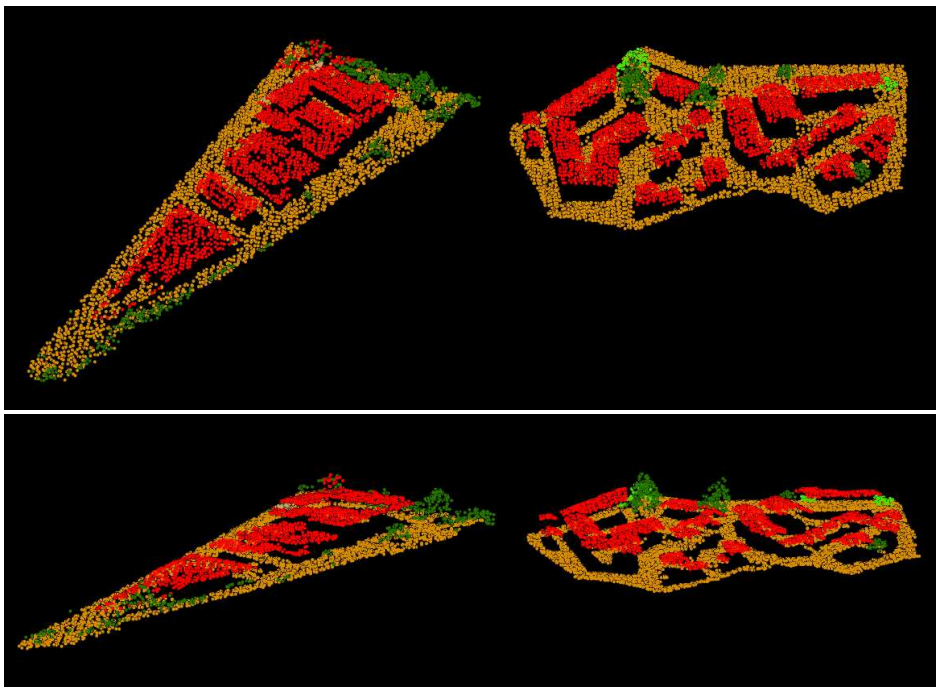

Figure 3.2: LIDAR's point cloud.

- to detect the vegetation the appropriate roughness value is 0.3 because the studying area is an urban area while mountain areas the roughness

can reach values 0.6. Beside the roughness, the areas with less than 50 points are considered of vegetation.

- 65 degrees is the maximum value of the slope roofs to classify the buildings , $0.65m$ the minimum high and 25 the minimum points of a building.
- for the classification of the ground are available two algorithms, one more suitable for urban areas and a second one for mountain areas. In this case is used the first one.

After the automatic classification it is necessary to perform a control and in some cases to manually edit small regions. "VRMesh Studio" provides a few tools that make this task easier so it is possible to classify few points let over from the automatic process and to recatalog some points that were listed incorrectly. As last and probably most important step some filter and interpolation remove the noise from the data. As well in this case after an automatic process a manual cheek to obtain a better result is important.

3.1.2 DSM

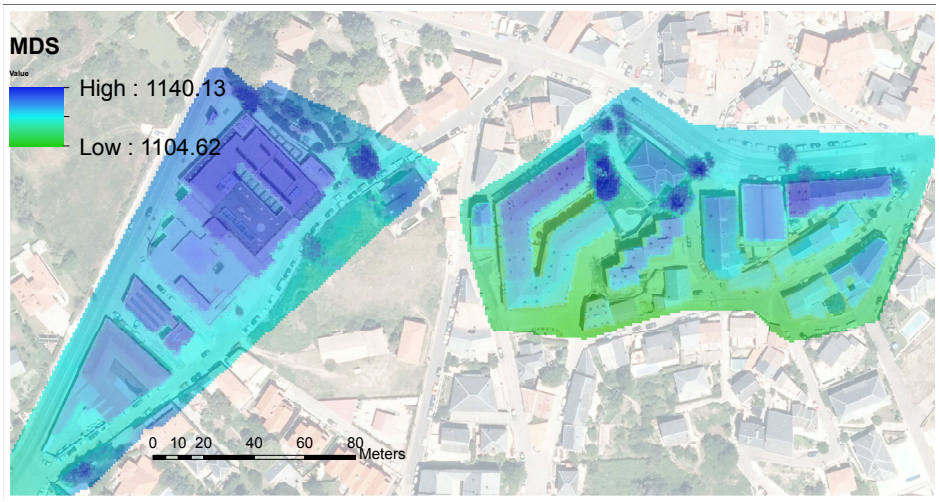

Figure 3.3: Digital surface model

After editing the LIDAR's data with ArcGIS 10.1 a digital surface model (DSM) of the urban area is crated the DSM allows taking into account the surface of the terrain and the form of buildings and trees. To calculate the DSM, from the cloud of LIDAR points first is fundamental to create a TIN

(triangulated irregular network). Subsequently the TIN is transformed into a raster using a conversion tool using the "natural neighbor weights" method of interpolation ensuring smooth surface but as well respect to the original position of the points.

As it will be explain later from the DSM will be calculate the local orientation and inclination. Here some results are anticipated only in order to see the quality of the DSM and to estimate his error. Three roofs with different characteristics are studied in more detail. The first roof is a flat roof with

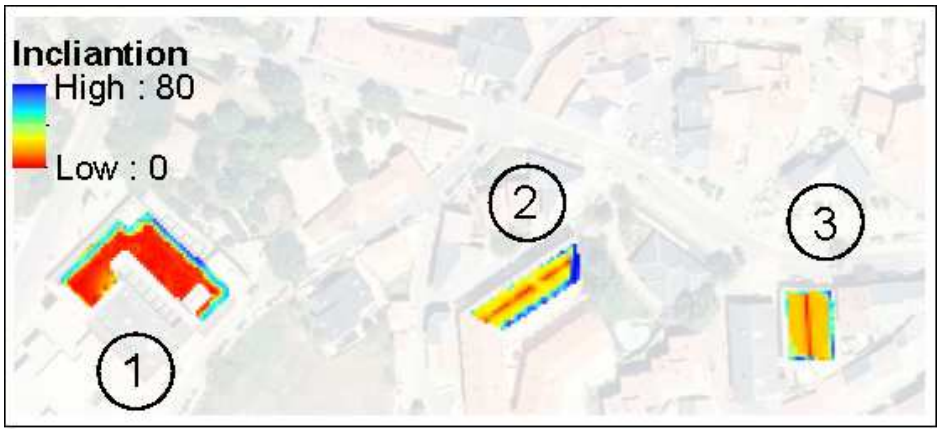

Figure 3.4: Inclination

complicate geometry, the second is a portion of a big building and the last one is the roof of a small house. The most critical points are the ones near a change of the slop as the ones along the perimeter of the roof and the ones on the top. Exuding this points the inclination is determinate in a range of $\pm 3^o$ (see Fig.(3.5)).

3.2 Determination of the utilizable surface

Once that an urban model is available, an important point is to calculate the surface where it is possible to place a PV panels. Whit the data from the "Dirección General de Catastro" (the Spanish land register) the buildings are discriminated. After is necessary to identify the useful part. In Fig.3.2 the idea is schematic represented. In this Section will be explained the first two filters based on the map of historical and relevant buildings and on the need to let a part of the roofs free. After the calculation of the irradiation's map the other two filters, the threshold for losses and for minimum area will be introduced.

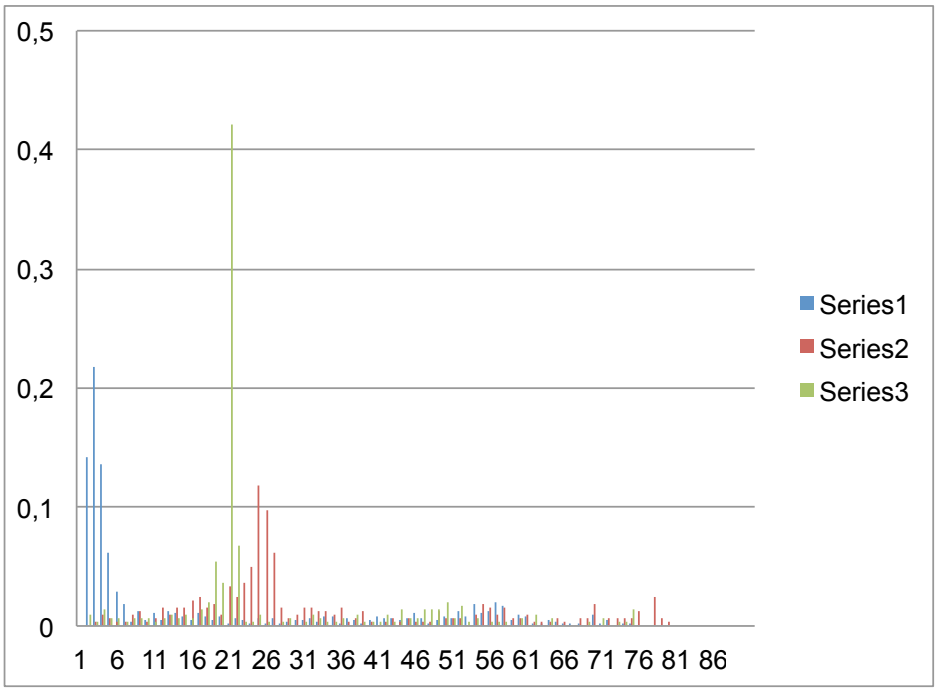

Figure 3.5: Distribution probability of the inclination in degrees of three roofs.

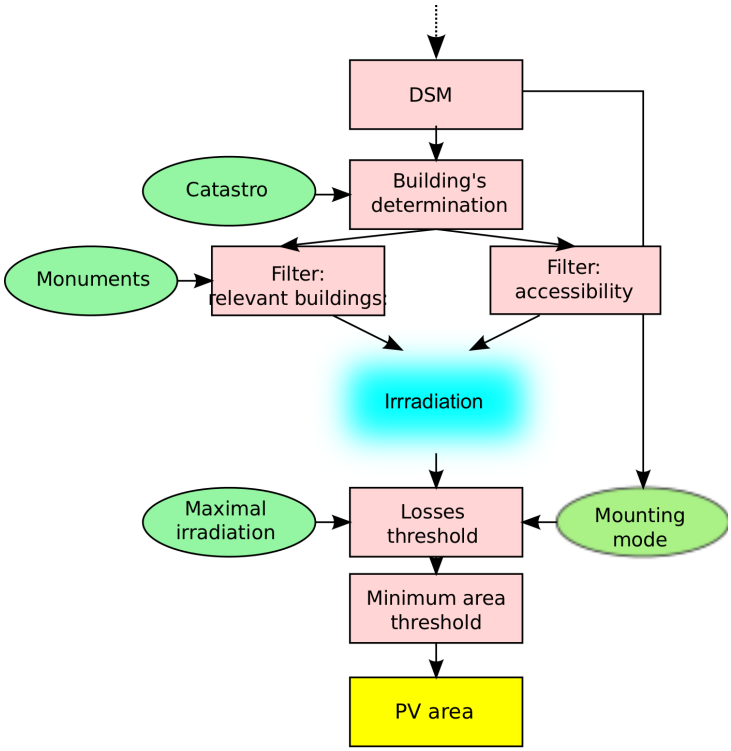

Figure 3.6: Schema of the determination of the utilizable surface.

3.2.1 Monuments and landmark buildings

In all urban areas there are buildings that for their historical significance or characteristics are not suitable for the installation of photovoltaic systems. Those buildings are identified and excluded it form the interesting buildings.

Although Miraflores de la Sierra is a municipality where the presence of these buildings is not very large, however it is necessary to take into consideration some of them. With respect to the selected study area there is no singular monument or building that must be taken into account but for more generality this criteria is also included in the model.

3.2.2 Accessibility to the roofs

On other important factor that has to be considered is the accessibility to the roof where the modules are located. These areas should facilitate maintenance of photovoltaic systems and access for firefighting. It is common to leave 1m from the perimeter of the roof.

In Fig.3.7 it shows the model to exclude this area form the roof's surface that can be used to install a PV system. The model first assigns to the buildings value 1 and value 0 depending if they are suitable for a PV system or not. After, this raster is combining with a raster where an area of 1 m wide around the rooftops is excluded. So at the end the surface where in principle it is possible to place PV system is obtained. Combined with the criteria of

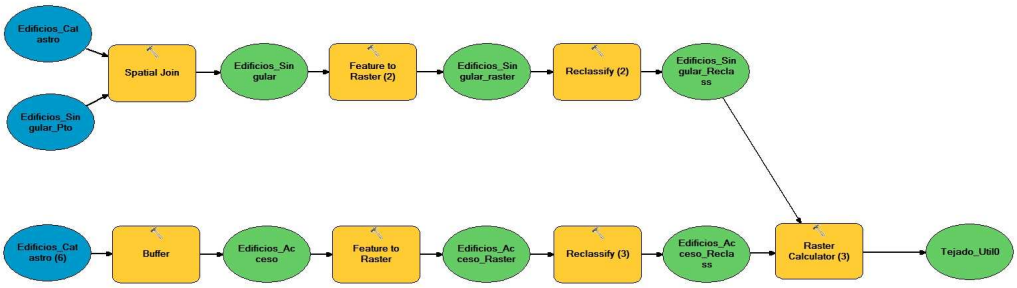

Figure 3.7: Model to identify relevant buildings and the accessibility to the rooftops.

exclusion of monuments and landmark buildings a first approximation of the useful surface is obtained.

Chapter 4

Solar irradiation

The production of electricity is directly related with the amount of solar radiation that the photovoltaic panels are able to capture. Therefore, one key point of our work is to knowing the amount of incident solar irradiation on the roof. It is necessary to know it over the whole year and for each point of the roof. The inherent difficulty is that the irradiation change at any point and at any time and obviously a direct measure it is impossible therefore it is necessary to develop an algorithm, based on standard method [22], to estimate the incident irradiation depending from the specific property of the roof (inclination, orientation and presence of shadow) and from the meteorological characteristics. One way to proceed is to start from the irradiation on a horizontal surface without shadow and then estimate the real irradiation on each point of the roof tacking into account the specific inclination and orientation and the presence of the shadow. Date of the global solar irradiation on a horizontal surface obtained with a statistical approach by satellite images [27] are used. This provides the hourly irradiation in a year. In a second step this data has been elaborated with the model of Hay and Davis [22]. In the following part of this chapter describes how to apply this model in order to calculate the irradiation incident on an arbitrary surface. The basic idea is that it is possible to decompose the total irradiation G in his three fundamental components: the direct irradiation B the diffuse one D and the reflected one R. These components are functions of the irradiation on horizontal surface and the angle between the sun and our arbitrary surface. Figs.(4.2) and (**??** report two example of the variation during the day of the total irradiation $G0$, the direct irradiation $B0$ and the diffuse one $D0$ on a horizontal surface. Is evident in Fig.(4.2) how during cloudy days the direct irradiation is almost zero and the total irradiation is almost entirely given by the diffuse component. Before the begin it is necessary to determinate

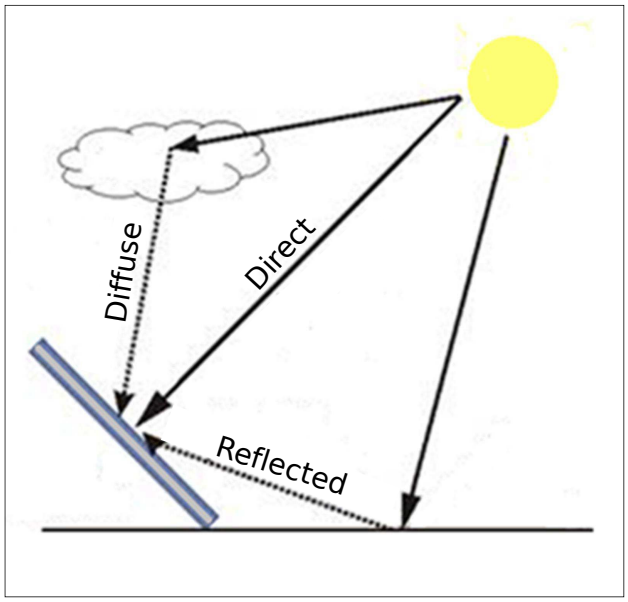

Figure 4.1: Decomposition of the radiation [figure adapted from [13]].

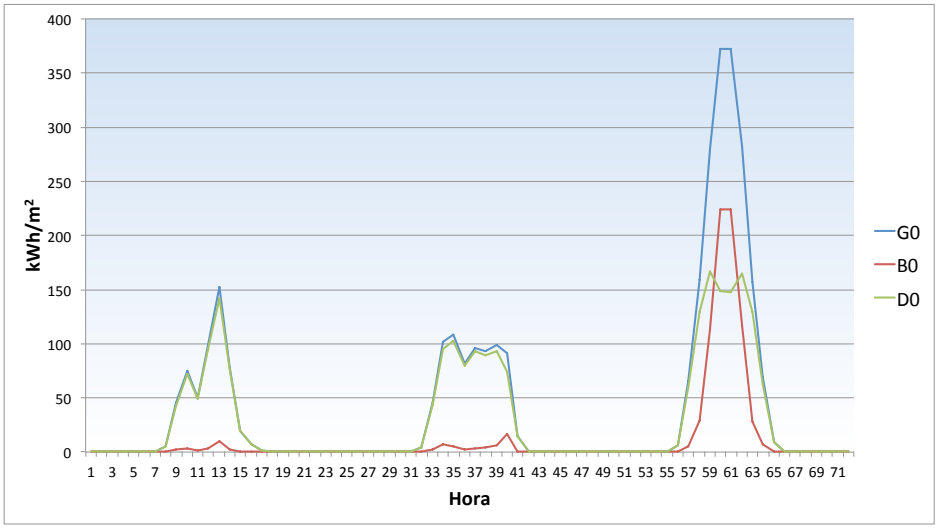

Figure 4.2: Evolution from the first to the third of January of the total irradiation on a horizontal surface $G0$ and his components: the direct irradiation $B0$ and the diffuse one $D0$.

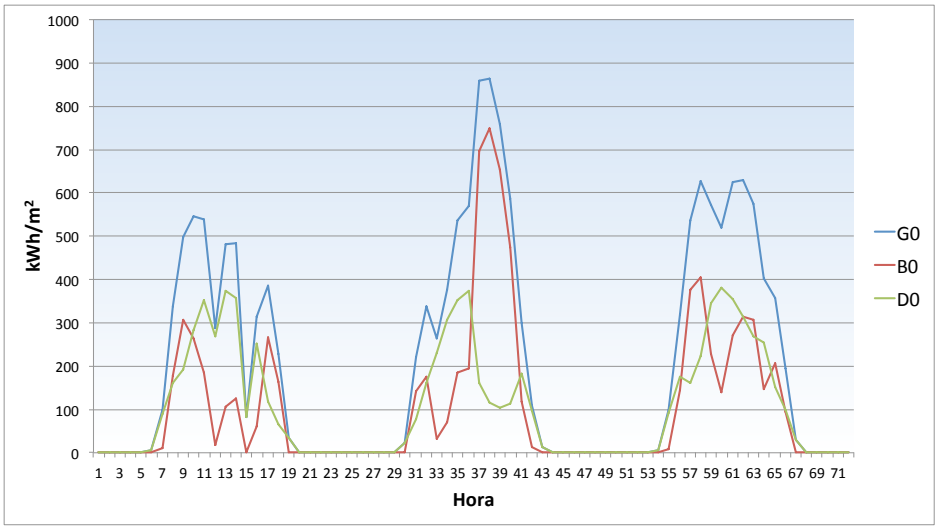

Figure 4.3: Evolution from the first to the third of May of the total irradiation on a horizontal surface $G0$ and his components: the direct irradiation $B0$ and the diffuse one $D0$.

the position of the sun during the year.

4.1 Position of the Sum

The position of the sun in a determinate moment of the day, is given by the declination of the sun δ and the solar hour angle, ω. The sun's declination is the angle between the plane of the Earth's equator and the line through the center of the earth and the sun. This angle is constantly changing, but its variation during a day is minimal, never exceeds the 0.5 degrees, so can be assumed that it is constant during the 24 hours of a day. The sun's declination is zero at the spring and autumn equinox. And during the winter solstice and the summer it reaches its maximum and minimum, respectively ($\delta = \pm 23,45 \text{degrees}$). Its value can be calculated by the following equation:

$$\delta = 23,24 \sin\left[\frac{360}{365}(d_n + 284)\right] \tag{4.1}$$

Where d_n is the day of the year and it is take between 1 and 365. In this equation the speed of the earth is approximate as constant during its elliptic orbit.

The solar hour angle has its zero at the solar noon and before solar noon

assume negative value, and after positive. The earth takes 24 hours to complete one revolution therefore so, one hour equals one angle of 15 degrees. The solar hour angle, for a given hour of the day is given by the following expression:

$$\omega = (12 - ET + AO - TO)15 - (LL - HH) \tag{4.2}$$

where AO is the official time-advance in Europe and it is one hour in winter and two in summer, TO is the official time, LL is the latitude of the local meridian, LH is the latitude of time and ET is the difference between the observable solar time and mean solar time. ET can be approximate by the, so called, equation of time:

$$ET = -7,64\sin(d_n - 2) + 9,86\sin[2(d_n - 80)] \tag{4.3}$$

The declination of the sun and the solar hour angle allows calculating the zenith angle trough the following expressions:

$$\cos(\theta_{zs}) = \sin(\delta)\sin(\phi) + \cos(\delta)\cos(\phi)\cos(\omega). \tag{4.4}$$

and the azimuth angle

$$\cos\psi_s = \frac{\cos\theta_{zs}\sin\phi - \sin\delta}{\sin\theta_{zs}\cos\phi} \tag{4.5}$$

The zenith and azimuth determinate the unitary vector pointing at the sun at any moment [Fig.(4.4)]. In Cartesian coordinate the unitary vector pointing at the sun is:

$$\begin{aligned} x_s &= \cos\theta_{zs}\sin\psi_s \\ y_s &= \cos\theta_{zs}\cos\psi_s \\ z_s &= \sin\theta_{zs} \end{aligned} \tag{4.6}$$

Finely, the value of the angle [Fig.(4.5)] between the sun and a surface with inclination α and orientation β can be written as:

$$\begin{aligned} \cos(\theta_s) = {} & \sin(\delta)\sin(\phi)\cos(\beta) - \sin(\delta)\cos(\phi)\sin(\beta)\cos(\alpha) + \\ & \cos(\delta)\cos(\phi)\cos(\beta)\cos(\omega) + \cos(\delta)\sin(\phi)\sin(\beta)\cos(\alpha)\cos(\omega) + \\ & \cos(\delta)\sin(\alpha)\sin(\omega)\sin(\beta) \end{aligned} \tag{4.7}$$

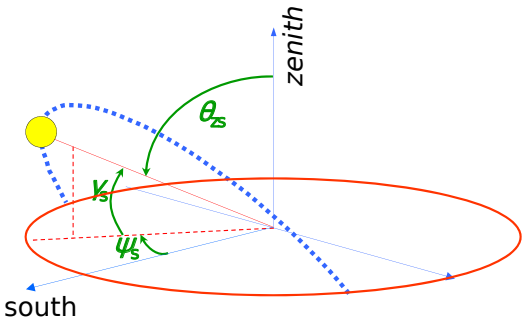

Figure 4.4: Schematic representation of the sun's position and his relatives angles. [adapted from [29]]

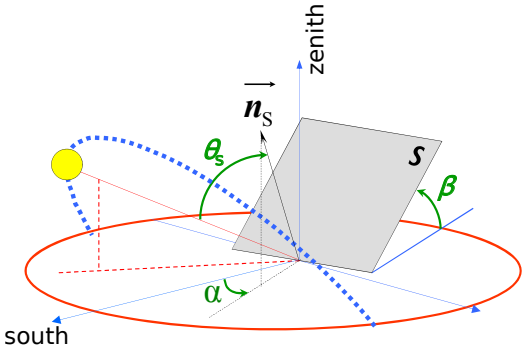

Figure 4.5: Panel's position.

4.2 Components of the global irradiation

Know the exact position of the sun and its reelection with an arbitrary surface, it is possible to calculate the hourly global irradiation on the surface. The global irradiation $G_h(\alpha, \beta)$ will be the sum of the direct irradiation, $B_h(\alpha, \beta)$, the diffuse irradiation $D_h(\alpha, \beta)$, and the reflected or albedo irradiation $R_h(\alpha, \beta)$. The index h represents the hour of year and goes from 1 for the one o'clock of first of January to 8760 for the midnight on 31 December.

Will now explained the way to calculate each of this three components following the Hay and Davis [22] model.

From simply geometric consideration the direct irradiation is given by

$$B_h(\alpha, \beta) = \frac{B_h(0)}{\cos \theta_{zs}} max\{0, cos\theta_s\} \tag{4.8}$$

In this equation the zenith angle and the incident angle correspond to the average value during the hour h.

The evaluation of the diffuse component and the reflect one is more complex. The diffuse component is due to the radiance that emits the whole sky with the exception of the solar disk. The difficulty is that the diffused irradiation is depending on the not uniform characteristics of the atmosphere. The irradiation distribution varies with the time and usually it is anisotropic. Only in the case of sky completely covered by clouds, the diffuse irradiation is isotropic.

In general it is possible to divide the sky in three different zone: an area circumsolar with some angular ξ_1 extension, and horizontal band with other ξ_2 angular extension and the rest of the celestial vault (which is assumed to behave as an isotropic irradiation emitter). Various models have been proposed to calculate the diffuse irradiation. A simplify version of the Perez's model assumes that all irradiation emitted by the circumsolar region, comes from a single central point (means $\xi_1 = 0$) and that the horizontal band coincide with the horizon (means $\xi_2 = 0$). So it is possible to express the diffuse irradiation as:

$$D_h(\alpha, \beta) = D_h^C(\alpha, \beta) + D_h^I(\alpha, \beta) \tag{4.9}$$

with the irradiation due to the circumsolar region

$$D_h^C(\alpha, \beta) = D_h(0) \left[k \frac{\cos \theta_s}{\cos \theta_{zs}} \right] \tag{4.10}$$

and the isotropic irradiation given by the sum of two terms corresponding to the horizon and the sky components.

$$D_h^I(\alpha,\beta) = D_h(0)(1-k)\frac{1+cos(\beta)}{2} \tag{4.11}$$

with the anisotropy index, $k = (G_h(0) - D_h(0))/(B_0\varepsilon_0 \cos\theta_{zs})$. And finally the reflected component can be approximated by

$$R_h(\alpha,\beta) = G_h(0)\rho\frac{1-\cos\beta}{2}. \tag{4.12}$$

In this case it is necessary assumed that the reflection of the environment is uniform. The behavior of the environment is described by the coefficient of reflection ρ that is 0 for a completely black and no reflecting object and 1 for a perfect mirror. The real urban environment is complex, with objects of different materials and shapes with very different reflection property but, it is assumed $\rho = 0,2$ as average coefficient of reflection taking into account principally the reflectivity of the tiles.

Using the three components given in Eqs. (4.9),(4.8) and (4.12) the total solar irradiation is given by:

$$G_h(\alpha,\beta) = B_h(\alpha,\beta) + D_h(\alpha,\beta) + R_h(\alpha,\beta) \tag{4.13}$$

This model and this equation are not taking into account the shadow and therefore this result is strictly valid only if there is no shadow on the surface. In the case that the surface is in shadow the total irradiation can be approximate at the first order as given by the sum of the isotropic diffused and the reflected components:

$$G_h(\alpha,\beta) = D_h^I(\alpha,\beta) + R_h(\alpha,\beta) \tag{4.14}$$

In this equation introduces a small error assuming that the reflection is the same as in the Eq.(4.13) because in the reality it should be taken into account that probably the shadow affect as well the environment in the proximity of the surface and therefore the reflected component is reduced. It is possible to neglect this effect because the reflected component is smaller than the diffusion component and therefore this correction are of the second order and don't affect strongly the result. The toolbox "hillshade" calculate which portion of the roofs are in shadow and then it is necessary implemented an algorithm that starting from the data of the hourly irradiation and using the equations explained in this section calculates the irradiation on the roofs. This process with more details will be explained in App.B.

Chapter 5

Optimization of the different kind of roofs

PV systems can be divided basically into three categories, depending on where there are situated, ground-mounted, roof-mounted and building-integrated. The ground-mounted systems are usually medium-big plants located on free fields outside the city. The PV panels are mounted on structure that can be static or mobile to allow solar tracking in order to maximize the production. A second possibility is to mount PV system on the top of building's roofs. Typically the size of this plant is medium or small and the solar tracking is not used. Although the location of the panels on the roofs and decks is pretty widespread option, in recent years have been developed systems that simultaneously act as architectonic structure and as photovoltaic systems to generate electricity. This system can be integrated in building elements as windows, overhangs, and skylight. The focus of this work on photovoltaic systems on roofs without considering the other two types.

Photovoltaic system on a roof can be placed with simple structure parallel to the roof or depending on the inclination and orientation of the roof, it can be opportune to mount the photovoltaic panels on a static structure that allow to dispose the panels on a particular inclination and orientation in order to maximize the energy production [see Fig.(5.1)]. We develop an approach capable to: (1) differentiate this two case and (2) calculate photovoltaic potential for panels with a disposition different from the one of the roof.

The photovoltaic potential is calculated in a general way so without introducing a specific type of panel with its dimension and properties. Therefore, in the DSM the real presence of the panels is not included (as done for example by other simulation tools as PVsyst). This leads that it is necessary to

Figure 5.1: Above, panels mounted parallel to the roof with a simple structure (from www.solarelectricsupply.com). Below panels mounted with an inclination and orientation different of the one of the roof itself (from www.mounts4solar.com)

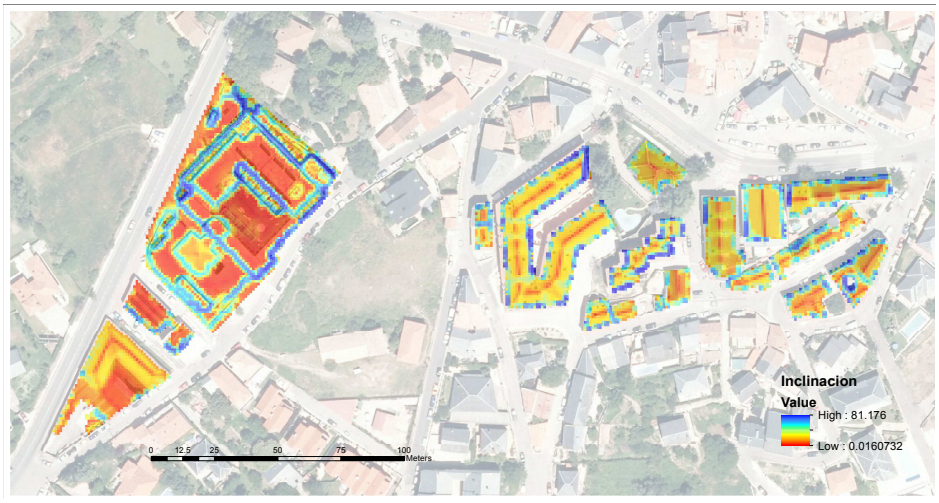

Figure 5.2: Inclination of the roofs.

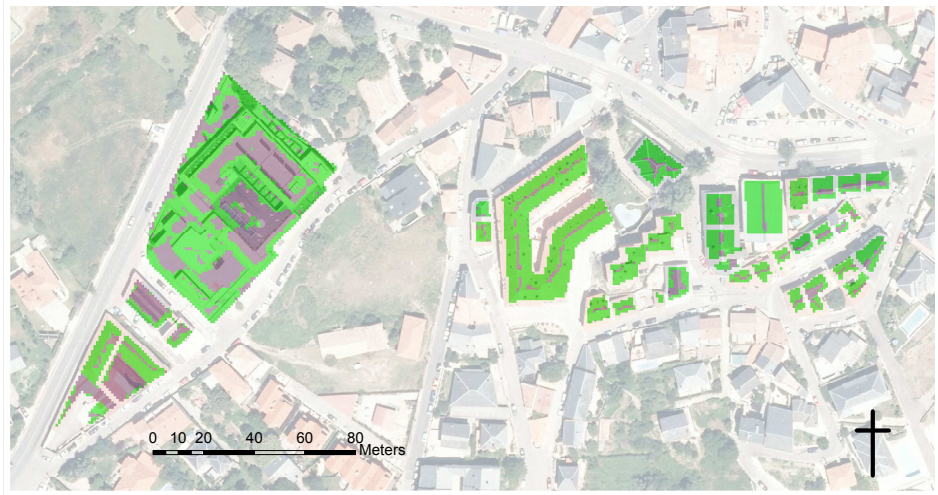

Figure 5.3: Two categories of roof: in green the one where the panels are mounted parallel to the roof and gray the one where the panels have different orientation and inclination.

take into account in an indirect way the presence of the PV panels. In particular it is necessary to deal with: the surface actually occupied by the panels, the estimation of the distance between lines of photovoltaic panels and the shadow that the panels generate. When the PV panels are just superposed to the roof as in the case of sloping roofs this three problems ere not relevant but they becomes fundamental if the PV panels are on a structure that disposes them with different angle and inclination compared to the roof on which they are located. After discussing which one is the "best" disposition and for a PV panel, in the following sections this three aspects are discussed in details.

5.1 Optimal disposition

The choice of the disposition of the solar panels is a very complicated task, it depends on many factors and it is not possible to give an always valid rule to apply. Generally the PV panels can be placed directly over the roof or using special structures that allow arranging them with the desired orientation and inclination The second solution is clearly the most flexible, however, is also the most expensive. So the first thing that has to be decided is if the higher cost of installation is offset from an increase in the productivity of the panels. If it's the case, it would be necessary to determine the optimal inclination

and orientation of the panels. This basically depends on whether hast to be maximize: the production respect to the panel's surface or the production respect to roof surface. Until recently, being the panels expensive, it was standard to maximize the production respect to the surface of the panels. Lately, the prices of the panels are considerably reduced therefore, in some cases, it may be more convenient to arrange the panels in a way that the production per surface of the panels is smaller but it is possible to mount more panels on the same roof in order to maximize the production of the single roof.

The choice of the best solution in each particular case is beyond the scope of our work so, the roof is divided in two general categories. The first category include all the roof that have an inclination less than 5 degrees and any orientation and the roof that have an inclination between 5 and 15 degrees and oriented to the south ($-90 < \alpha < 90$). In this case these types of roof are simply called "flat" and the panels are inclined and orientated at the optimum. In any other case, for the "sloping" ones, it is not convenient to mount additional structures then the orientation and inclination of the roof and the panels will be the same. And for the roof of the first category the optimum coincides whit the maximum of the production respect to the surface of PV panels. The following part of this chapter explains the reason of this decision and how to determinate the optimal inclination and orientation.

Roof's disposition	Roof's type	Panel disposition
$0 < \beta < 5$ $-180 < \alpha < 180$	flat	$\beta_p = 32$ $\alpha_p = 0$
$5 < \beta < 15$ $-90 < \alpha < 90$	flat	$\beta_p = 32$ $\alpha_p = 0$
$15 < \beta$ $-180 < \alpha < 180$	sloping	$\beta_p = \beta$ $\alpha = \alpha$
$5 < \beta < 15$ $\lvert\alpha\rvert > 90$	sloping	$\beta = 32$ $\alpha = \alpha$

Table 5.1: Roof's classification.

The orientation is simply the south ($\alpha = 0$) in the north hemisphere and north in south hemisphere. To estimate the inclination, in the literature, there are different ways. The easier one it is just to use the equation $\beta_o = \phi - 10$ but this is not valid at low latitudes. A bit general equation is

$$\beta_o = 3,7 + 0,69\phi \tag{5.1}$$

and for the latitude of Miraflores it takes the value $\beta_o \approx 32$. Instead of using these approximate expressions it is better to use the equation for the irradiation [Eq.(4.13)], from this equation it is possible to calculate the irradiation at any inclination and therefore, to determinate which is the best inclination for the panels and estimate the loss if the panels have a different inclination and orientation. The irradiation has a flat maximum at $\beta = 32$ [see Fig(5.1)] that confirms what obtained with the two previous expressions.

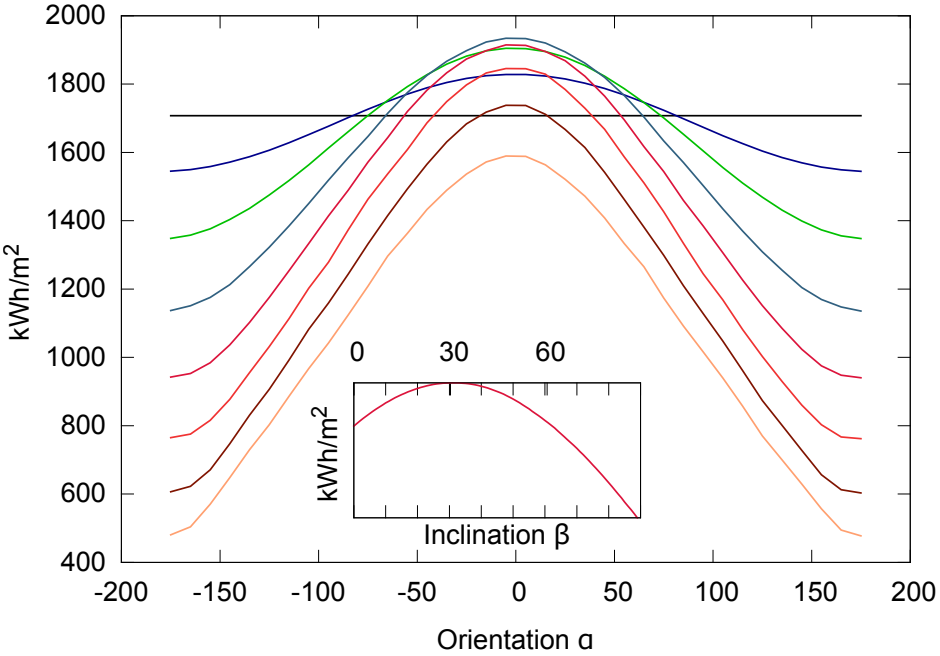

Figure 5.4: Total irradiation in one year as function of the orientation α. The different lines are for different value of the inclination β. The horizontal one is for a horizontal surface and then other are for $\beta = 10$ to $\beta = 90$ at step of 10 degrees. In the inset the total radiance as function of β for $\alpha = 0$ is plotted.

5.2 Effective surface

The first aspect to take into account is that a tilted panel occupies an area of the roof less than its own surface. This can simply consider with the geometric factor

$$C_f = \frac{1}{\cos(\beta_o - \beta)} \tag{5.2}$$

that is simply the projection of the length of the panel with inclination β_0 on a roof with inclination β (see Fig.5.2) .

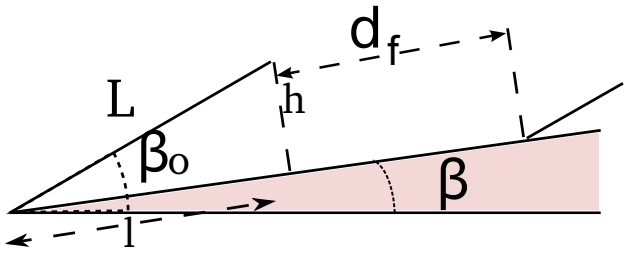

Figure 5.5: Geometry of a panel.

5.3 Optimal distance between lines

The second issue that has to be discussed is the distance between rows of PV panels. If there are different rows of PV panels it is important to analyze the shadow that each row creates on the next row. Then greater the distance between the rows is, the smaller the number is of hours in a year in which the panels are covered by the shadow of an eventual before row. However, increasing the distance decreases the number of rows that can be arranged on a given surface. There are several works that discuss how to define the distance between the rows according to whether you want to optimize the production in relation to the surface of the roof or of the PV panel. Using the

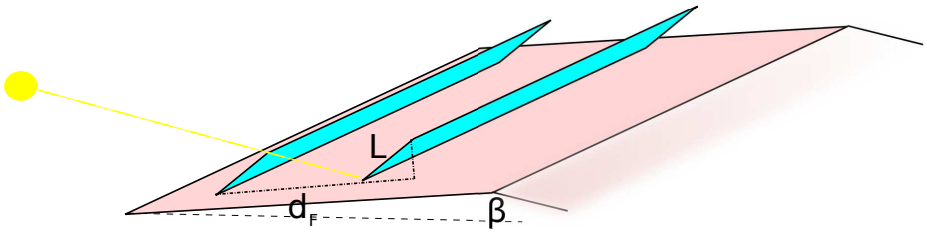

Figure 5.6: The optimal distance between lines

common rule to avoid shadow during the solar winter noon so the distance between lines of panels is:

$$d_F = \frac{h}{\tan(61 - \varphi + \beta)} \tag{5.3}$$

$$= L\frac{\sin(\beta_o - \beta)}{\tan(61 - \varphi + \beta)} \tag{5.4}$$

The ratio between the the PV panel's surface and the roof's surface necessary to install the panel i.e, the sum of the projection of the length of the panel on the roof l and the surface of roof that has to be let free as distance from the next row d_F (Fig.5.5), is:

$$C_d = \frac{L}{l + d_f} = \frac{1}{\cos(\beta_o - \beta) + \frac{\sin(\beta_o - \beta)}{\tan(61 - \varphi + \beta)}}. \tag{5.5}$$

This factor allows considering the actual use of the roof.

5.4 Shadow

The last aspect that has to be discussed is the shadow generates form the PV panel. Shadow plays an important role in the design of photovoltaic system. Although solar panels can operate with diffuse irradiation the presence of shadow reduces significantly the amount of energy produced by a panel. In some extreme conditions shadow can reach to damage the panels themselves by creating "points of fire"; although in most modern panels, this risk is greatly diminished thanks to the use of diodes.

The shading analysis must consider different elements like the topography of the land, rooftops and adjacent buildings, wooded areas, walls or other surrounding element. The "Hillshade" tool included in ArcGIS determines the illumination of an area from the raster surface model taking into account the position of the sun. This allows to estimate whether an area is shaded or not and the size of the shadows at a given time. In this way the shadow on the roof is calculated and can be assumed that this coincides with the shade slicing the panels positioned above it. Clearly this is an approximation because the surface of the panels will be a little above than the surface of the roof itself, and then the shadow on the panels will be smaller. Since the distance between the surface of the roof and the surface of the panel is small and the difference between the two shadows is especially big in case of poor irradiation (for example, when the sun is low above the horizon) this approximation can be safely used. Moreover, as we will see later, we are underestimating the effect of the shadow on the production of energy, so in a certain way the overestimation of the dimension of shadow compensates it.

In the case of flat roofs with the panels disposed in various rows, a row can cast its shadow on an other row. The "Hillshade" tool is based on the DSM where, the structures of tilted panels are not present. Therefore, it is necessary to develop an additional tool in order to calculate the shadow

generated by the presence of the panels. Knowing the disposition of the panels and the position of the sun during the year with some geometry it is possible to calculate if in a particular moment a line of panel casts a shadow to the next line.

Let begin looking at the simple case of a flat roof oriented to south ($\beta = 0, \alpha = 0$) and let assume as first approximation that the rows have infinite length. This approximation overestimates the effect of the shadow. The length of the shadow in this case is given by:

$$L_S = L\left(\cos\beta + \frac{y_s}{z_s}\sin\beta\right) \tag{5.6}$$

with y_s and z_s the sun's coordinates (see Eqs.(4.6)). If $L_S > L\cos\beta + d_F$

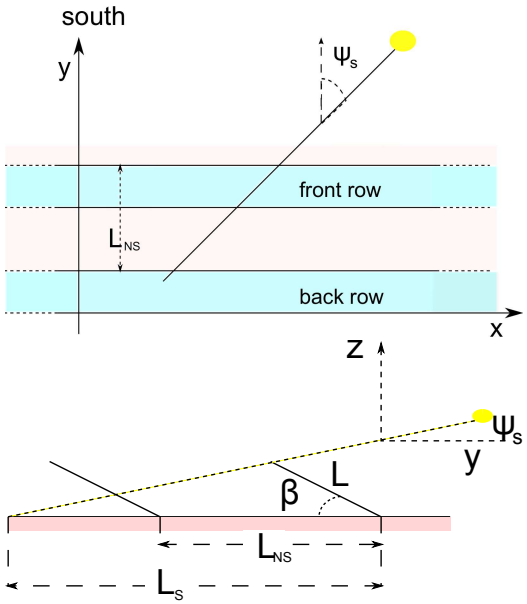

Figure 5.7: Shadow created by parallel line of panels.

the back row is in shadow and the fraction of his surface in the shade, the so-called shadow factor, is[30]

$$S_f = 1 - \frac{L_{NS}}{L_S} \tag{5.7}$$

, whe L_{NS} is showed in Fig.(5.7) that can be written in a general way as:

$$S_f = max\left[0, 1 - \frac{\cos\beta + d_F}{\cos\beta + \frac{y_s}{z_s}\sin\beta}\right]. \tag{5.8}$$

It is possible to reduce any case where the roof as a different orientation ($-180 \leq \alpha_{tejado} \leq 180$) and inclination ($0 \leq \beta_{tejado} \leq 90$) to this result performing a rotation of α_{tejado} around the $z-$axis and one of β_{tejado} around the $x-$axis. The rotations are given by the unitary matrices:

$$T_z = \begin{pmatrix} 1 & 0 & 0 \\ 0 & \cos(\beta_{tejado}) & -\sin(\beta_{tejado}) \\ 0 & \sin(\beta_{tejado}) & \cos(\beta_{tejado}) \end{pmatrix} \tag{5.9}$$

and

$$T_x = \begin{pmatrix} \cos(\alpha_{tejado}) & -\sin(\alpha_{tejado}) & 0 \\ \sin(\alpha_{tejado}) & \cos(\alpha_{tejado}) & 0 \\ 0 & 0 & 1 \end{pmatrix} \tag{5.10}$$

With this transformation the position of the sun in the new reference system is given by:

$$\begin{pmatrix} x_s'' \\ y_s'' \\ z_s'' \end{pmatrix} = T_z T_x \begin{pmatrix} x_s \\ y_s \\ z_s \end{pmatrix} \tag{5.11}$$

Therefore in a general case the shadow factor is given substituting in Eq.(5.8) the position of the sun in the new coordinate (Eq.(5.11)). This equation is not valid if $y_s'' < 0$ when the sun illuminate the back of the photovoltaic panels and therefore the shadow factor can be consider equal to 1. And as well if the sun is hidden by the roof surface ($z_s'' < 0$), $S_f = 1$. As said before this equation is not exact for rows with finite length λ. But it is possible to calculate a correction $S_{SN} = S_f * K$ to take into account this:

$$K = max\left[0, 1 - \frac{L_{SN} - \cos\beta}{\lambda}\frac{|x_s''|}{y_s''}\right]. \tag{5.12}$$

This correction factor is smaller than 1 ($L_{SN} - \cos\beta = d_F > 0$), therefore not taking it into account overestimates the effect of the shadow and underestimating the irradiation received by the panels and namely, the energy produced. Over the year this correction is secondary because, it is non-zero only in the early hours of the day and during sunset, especially in the winter when the PV panels produce just a small fraction of the total electricity.

5.5 Conclusion

As it is impossible a case-by-case analysis in this chapter a method in two steps to decide the layout of panels on a roof has been established. First the roofs are divide into two categories, in the first panels will be mounted parallel to the roof and in the second they will be arranged through structures with the desired inclination and orientation. The second step is to decide the orientation and inclination for the panels of the second category. As explained above, this depends on what we want to optimize. In this work has been chosen to maximize the annual radiation captured by the panel surface. In this case, the optimum inclination turns out to be of 32 degrees. Otherwise it will be possible to use a lower inclination, so that the radiation captured by the single panel would be lower, but would be possible put a larger number of panels in the roof. Indeed reducing the angle, the distance between panels [Eq.(5.3)] becomes smaller.

It is interesting to study this with the help of the equation developed up to here. The factor of exploitation of the roof may be calculated by $F_u = L/(l + d_F) = C_d$, the ration between the surface occupied the paneles and the surafce of the roof.

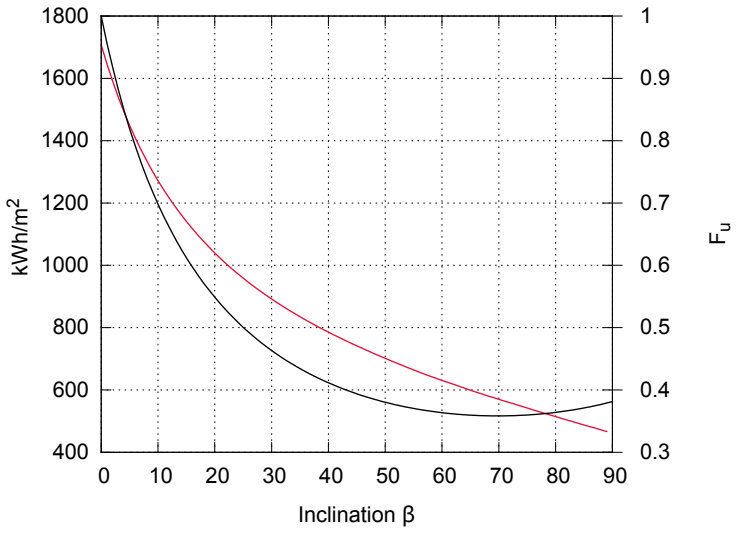

Figure 5.8: Irradiation per square meter of the roof (red line) and the exploitation's factor (black line) as functions of the inclination of the panels β

The ration between the total irradiation on a roof and the surface of the roof itself (irradiation per square meter of roof) is highest when the

panels are arranged parallel to the roof becouse in this case the distance between the rows is 0 and it reduces increasing the angle of inclination [red line in Fig.(5.8)] when increases the distance between the rows [see Eq.(5.3)]. However, the radiation does not simply follows the trend of the F_u factor because the radiation increases until reaches an inclination of 32°.

Chapter 6

Solar potential

The calculation of the solar potential's map is based on three pillars: first the model of the irradiation [Sec.4.2], second the DSM [Sec.3.1.2] and third the shadow's model [Sec.5.4 and Ap.(A)]. How pictured in Fig.(6.1)

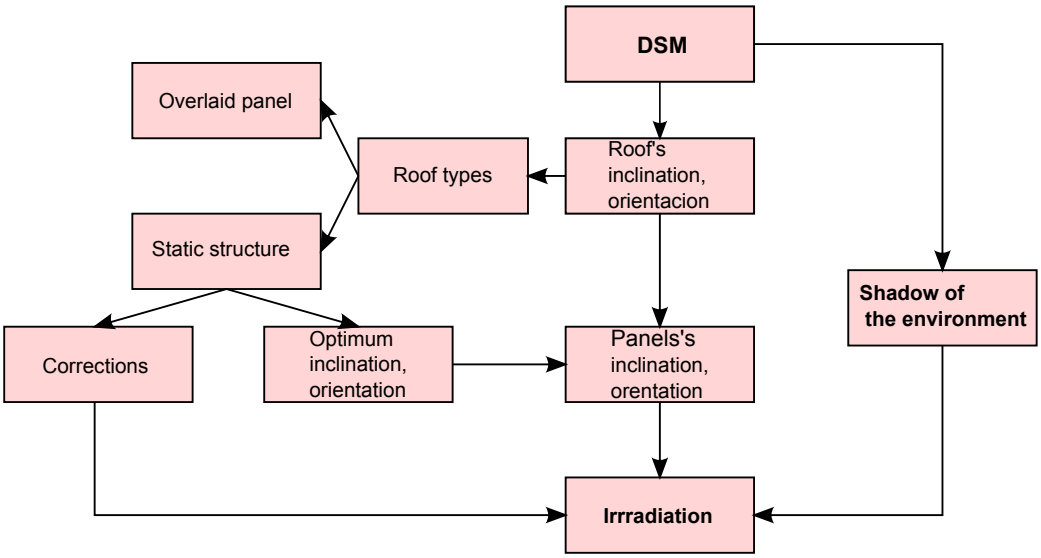

Figure 6.1: Schema of the irradiation's map

the DSM permits to obtain a map of the shadow [see Ap.(A)] and to know the inclination and orientation of the roofs. With this information the roofs are classified under the two categories introduced in Ch.(5). For "sloping" roof (if the inclination β is bigger the 15 degrees) it is convenient to mount the PV panels directly on the roof, then the inclination and orientation of the PV panels will be the same as that one of the roof. For "flat" roof

with $(5 < \beta < 15)$ and oriented to the south $(-90 < \alpha < 90)$ or $(\beta < 5)$ it is assumed that the PV panels are oriented to the south an inclined at the optimum inclination $\beta_o = 32^o$ [see Tab.(5.1)]. The roofs "nearly flat" $(5 < \beta < 15)$ but oriented to the north $(-180 < \alpha < -90$ and $90 < \alpha < 180$) are considered of the category of sloping roofs, because in this case usually it is not opportune to mount the panels on a particular structure. It is necessary to say that this type of roofs hardly pass the selection explained in Section (7.1), since the losses for orientation will be high. However, in principle, it cannot be excluded a priori without checking if it fulfils the requirements of minimum radiation.

The result is a map of the inclination and orientation of the panels different from the map of the inclination and orientation of the roofs. Finally this map and the shadow map will used as the inputs of the irradiation's equations [Eqs.(4.13)-(4.14)]. Furthermore for the "flat" roofs it is necessary to take into account the correction's factors explained in the Ch.(5).

To reduce the calculation time at this step the range of the inclination and orientation in the fields of 5 degrees is divided. This allows grouping many points of the roof's raster and significantly reducing the times to compute the radiation's map. This simplification introduces an error in the calculation of the radiation which is not very important since changes of 5 degrees in the orientation of the panels involving a change not exceeding 2% in the radiation received. It should also keep in mind that this simplification is concordant with the uncertainty in the determination of the orientation and inclination from the LIDAR data available to us (see section 3.1.2). On the other hand this simplification is necessary in case the area of study is large, such as entire cities. The details of how has been optimizing the algorithm is in Ap.(B).

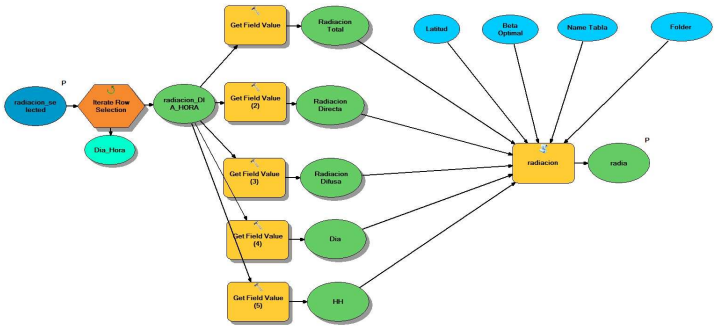

Figure 6.2: Radiation's model.

With this information a map of the irradiation $\bar{I}_g^h$ pro square meter of

roof is calculated using the equation:

$$\bar{I}_g^h = \bar{F}\, G_h(\alpha, \beta) \tag{6.1}$$

where the index h reminds that this are hourly data. $G_h(\alpha, \beta)$ is the total irradiation given by Eq.(4.13) and by Eq.(4.14) in the presence of shadow. $\bar{F}$ is a factor related to the two types of roof, it is equal to 1 for "sloping" roof and $\bar{F} = C_d(1 - S_F)$ for "flat" roof.

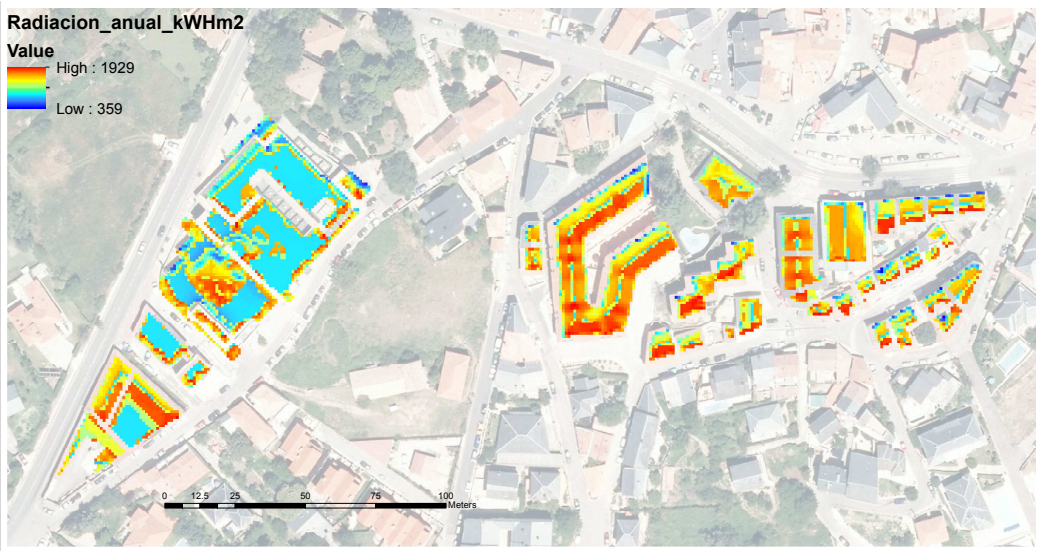

Figure 6.3: Annual irradiation in kWh pro square meter of roof.

Once obtained the hourly irradiation it is enough to sum over a year to obtain the total annual irradiation map. In Fig.(6.3) are reported the results. Depending on the type and the sloop of the surface the value of the irradiation is going from $360kWh/m^2$ to $1930kWh/m^2$. The maximum it is reach for roof oriented to the south with an optimum inclination and not affected by shadow during the whole year. PVGIS gives an annual irradiation on optimal inclination of $1890kWhm^2$ value that agrees with our result. On flat roofs has a lower value $I_g \approx 1300kWh/m^2$, because on this roofs the panels are mounted in rows with a certain distance distance in order to avoid unwelcome shadows. Looking at the irradiation pro square meter of PV panel

$$I_g^h = F\, G_h(\alpha, \beta) \tag{6.2}$$

where F is equal to 1 for "sloping" roof and $F = (1 - S_F)$ for "flat" roof, it is evident the advantage to place the panels on flat roof on the optimal inclination and orientation [Fig.(6.4)].

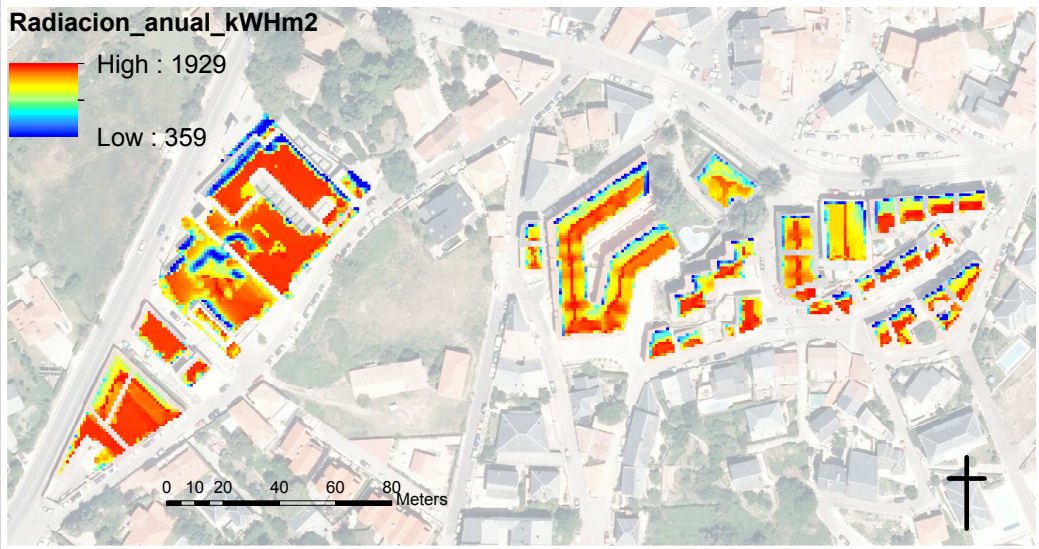

Figure 6.4: Annual irradiation in kWh pro square meter of PV panel.

In Fig.(6.5) there is an example of how the shadow of different elements like three, rooftops and adjacent buildings affect the radiation. In this case on the roof there is an object (in the red circle) that in the early morning cast his shadow on a portion of the roof and therefore in this area the radiation is lower.

In generally, excluding small portions the irradiation is pretty uniform, this is due to two factor. First, the absence of high buildings or three that cast relevant shadow on the roofs. During the central hour of the day the roofs are almost fully enlightened by the sun [see Ap.(A)]. The shadows affect the roofs only in the hours when the sun is low and therefore only as a small fraction of the total annual irradiation is missed. Second, many roofs have low inclination (around 20 degrees) therefore the amount of irradiation received is not strongly affected by the orientation. A inclination of 20 degrees is the case of the green line in Fig.(5.1) that almost reach the 1900 kWh/m^2 and his minimum is 1350 kWh/m^2, with a maximum variation of the 30%.

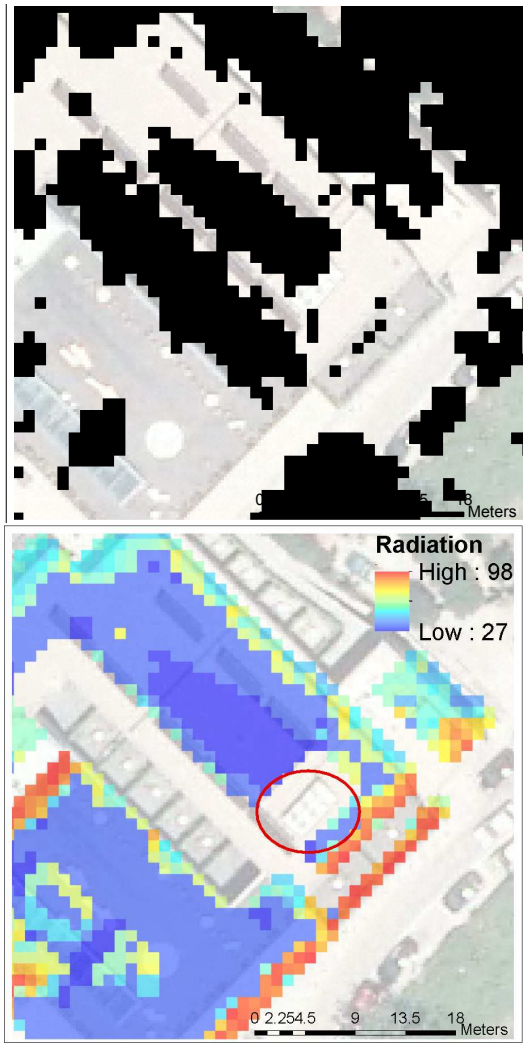

Figure 6.5: In the upper figure there is the shadow on the roof. Below the radiation on the same roof.

Chapter 7

Determination of the suitable surface

To calculate the surface suitable to place a PV system is an important goal of this work. At the begin the whole surface of the city is considered after several criteria eliminate the areas that are not usable. First the data from the "Catastro" (the Spanish land register) discriminate where the building are. Second the relevant and historical buildings are excluded, and as well perimetric area that has to be free for maintenance or in case of fire. Now with the map of the solar potential is important to select the part of the roofs where it is really convenient to install PV panels, this depends on the amount of solar radiation that a PV panel can receives in a determinate place. As last the areas that are too small are excluded. This chapter analyzes the last two criteria.

7.1 Irradiation threshold

The selection process of the suitable roofs is not unique. This work takes into account the technical specifications of the "Pliego de Condiciones Técnicas" (CTE) specified in the basic document HE5 about energy saving.

	Orientationand Inclination	*Shadow*	*Total*
general	10%	10%	**15%**
superposition	20%	15%	**30%**
integration	40%	20%	50%

(7.1)

This document gives an indication of the maximal loss due to the specific location of the PV panels (orientation, inclination and shadow) respect to the optimum. If these losses are too large panel's installation is not convenient. The PV panels are divide in three categories: if they are mounted on specific structure, if they are mounted directly on the roof, or if they are integrate in the architecture of the buildings. And depending the categories the CTE specifies a maximum loss due to orientation and inclination and shadow. There are different approaches to calculate those losses. In the work [13] an empirical method was used. To calculate the effect of shadow, the region affected by shade during the four central hours of the day (10a.m. to 2p.m.) on any day of the year was excluded. Instead, to calculate for losses due to inclination and orientation was used the formula [31]:

$$P(\%) = \begin{cases} 2.5 * 10^{-4} * (\beta - \beta_o)^2 \\ 2.5 * 10^{-4} * (\beta - \beta_o)^2 + 3.5 * 10^{-5}\alpha^2 \end{cases} \tag{7.2}$$

This formula is quite good only for small variations respect to optimal values and generally these empirical approaches tend to overestimate the losses to guarantee a margin of safety, a step forward respect to this has been done in this work. Te maximum of the annual irradiation that a panel can receive is given by

$$I_{MAX} = \sum_h I_g^h = \sum_h G_h(\alpha = 0, \beta = \beta_o) \tag{7.3}$$

Calculating the global loss at each position respect to this optimum allows a more accurate estimation of the portion of the roof that is suitable for the installation of a PV panels.

This work takes into account only panels of the first two categories in the table 7.1 and does not differentiates between losses for tin inclination and orientation and for shadow so, the threshold are 15% and 30%.

In the area of study due to the low inclination of the roof, and therefore weak dependence of the irradiation on the orientation, and absence of strong shadow, the area that not pass the threshold for loss is relative small and certainly smaller then if the empirical method [13] is applied.

7.2 Area threshold

The last criteria that is for a minimum of area. After using the previous criteria small isolated areas can be regarded as usable but in reality they can hardly be used to place a PV system because they are too small. Therefore,

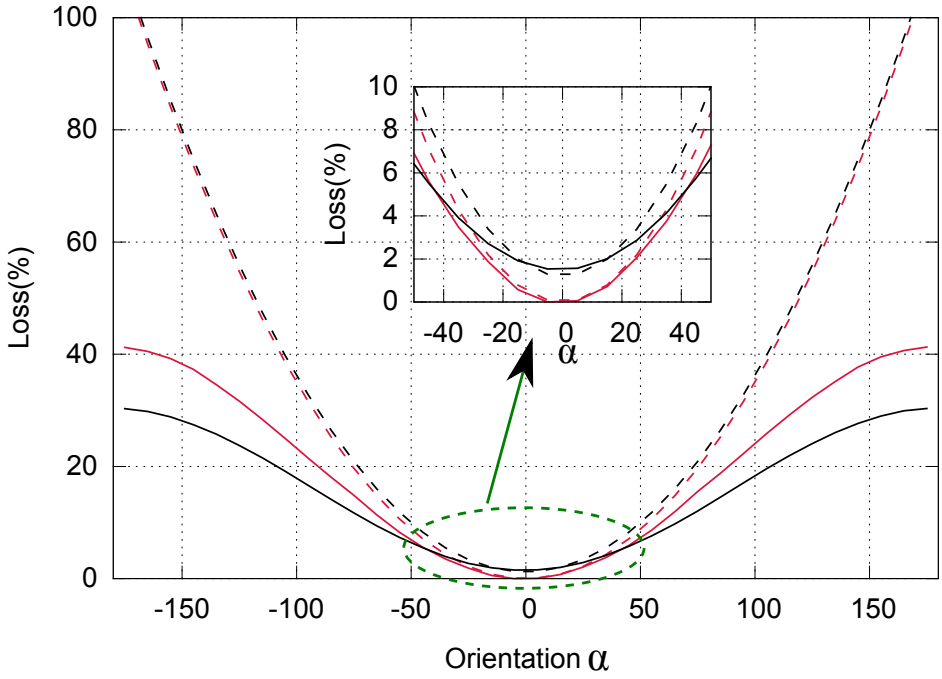

Figure 7.1: Loss due to the orientation for $\beta = 30$ (red) $\beta = 20$ (black). The dashed lines are obtained with Eq.(7.2) and the continue lines with our direct approach. It is clear that the empirical expression it is valid only for orientation near the optimum and otherwise leads to an overestimation of the losses and therefore to wrongly neglect big portion of the roofs.

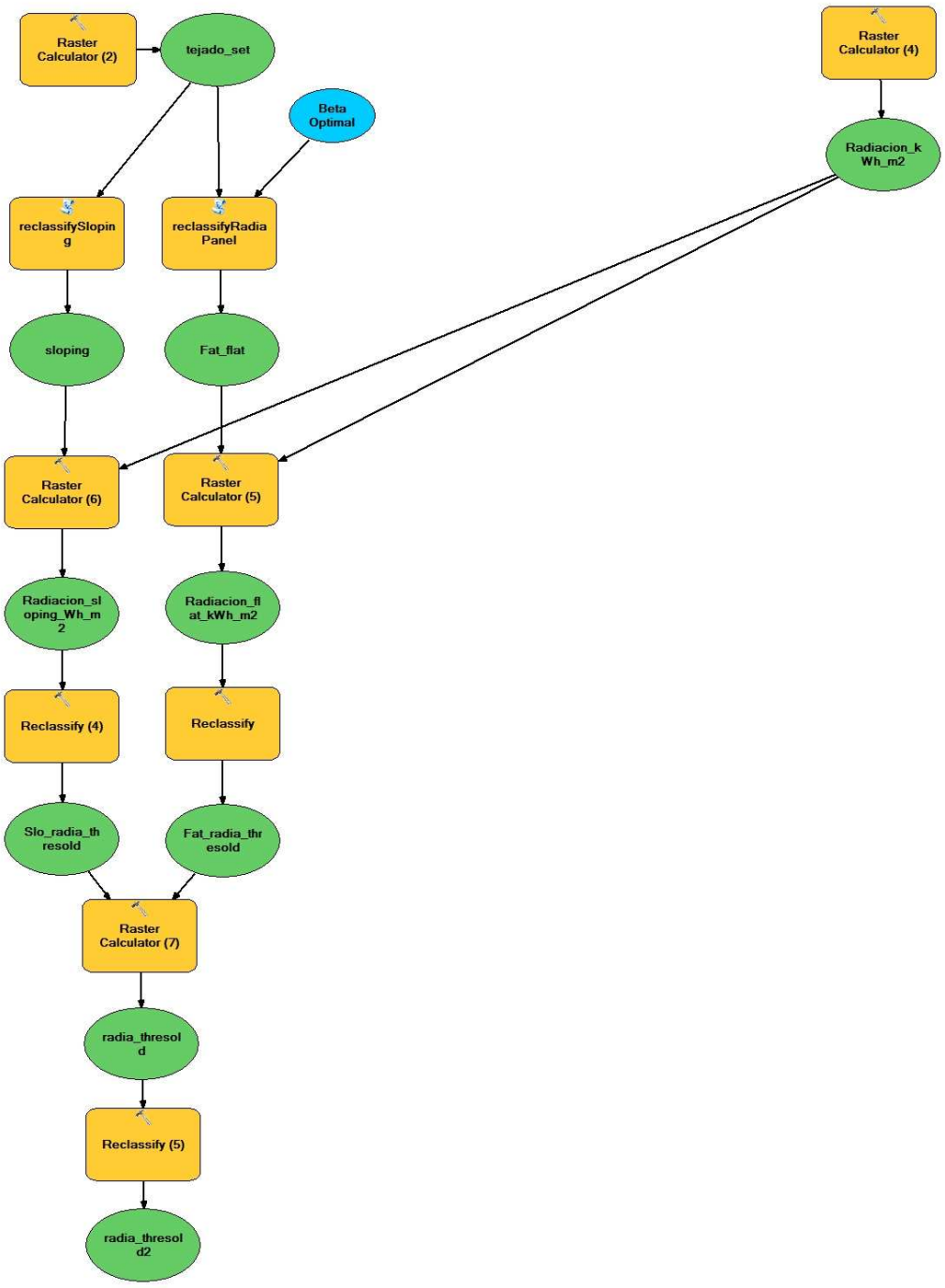

Figure 7.2: Model of irradiation threshold: depending on the typology of the system, roof with loss due to inclination, orientation and shadow more than 15% or 30% are neglected.

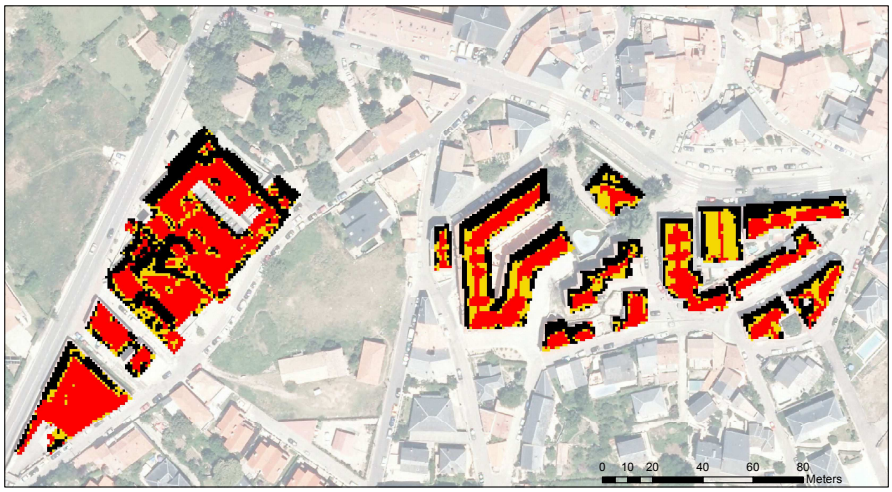

Figure 7.3: On black the areas where the annual irradiation is less than the 70% of the maximum, yellow where is between 70% and 85% and red where the irradiation is more than the 85%.

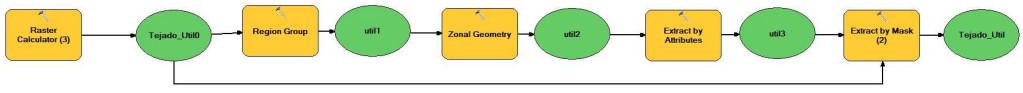

Figure 7.4: Area threshold's model

an algorithm discriminates these areas and eliminates them from the surface usable.

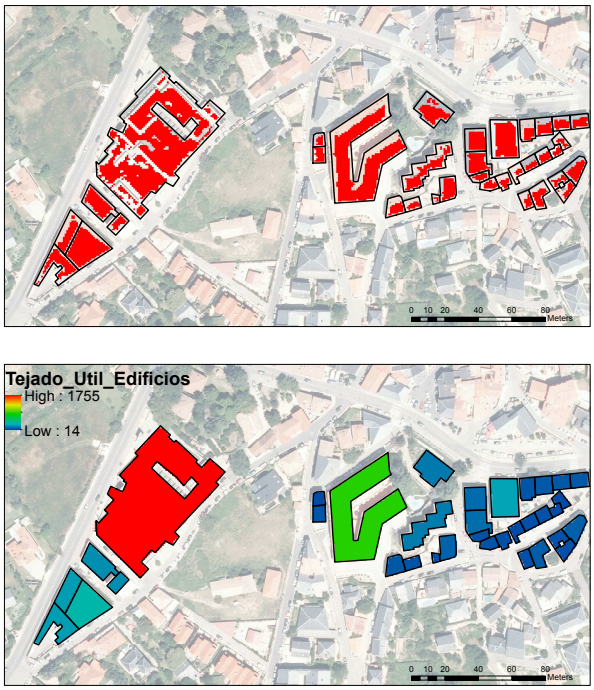

Figure 7.5: Above, in red the suitable part of the roofs. Below, the area in m^2 that can be used for each building.

The Fig.7.5 shows the portion of the roofs that can be used, taking into account the occupation factor C_d [Eq.(5.5)] it is possible to calculate the surface of the Pv pannels A_{PV}.

Chapter 8

Estimation of production

The effective annual energy production is given by:

$$E_{annual} = A_{PV}\, e \sum_h PR_h\, I_g^h \tag{8.1}$$

where I_g^h [Eq.(6.2)] is the hourly irradiation , e the efficiency, A_{PV} [Sec.7] the area of the PV panels and PR_h performance ratio. This chapter introduces the efficiency and the performance ratio. These depend on the type of the PV panel and on the installation. Almost all the panels on the market are fundamentally of two technologies: crystalline silicon or thin films. In Tab.(8) are summarized a few important differences between the two technologies [for more details see [32, 33]. The crystalline silicon panels are the most common, they ensure good efficiency and high reliability but are quite expensive and their behavior at high temperatures is not optimal.

	Si-c	**Thin films**
Technology	Mono and multi	many
Power (Wp/module)	200-300	40-360
Power (Wp/m^2)	120 -190	50-100
Loss of power with temperature ($\%/^oC$)	0.4-0.5	0.1-0.3
Open circuit voltage (V)	21-65	50-240
Short circuit current (A)	4-8	1-6
Dimensions (m)	1.64x1	highly variable
Weight (g/W)	60-100	160-340

Table 8.1: Properties of PV panels [33]

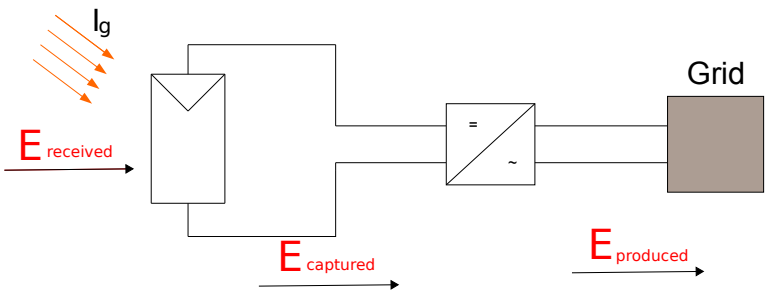

Figure 8.1: Schema of the installation. A panel receives an amount of energy $E_{received}$ depending on his location, only a fraction of this energy is transformed into electrical energy $E_{captured}$ and finally a part of this is fed into the grid.

On the other hand, the main advantage of thin films is their relatively low consumption of raw materials; high automation and production efficiency; easy of building integration and improved appearance; good performance at high ambient temperature; and reduced sensitivity to overheating. The current drawbacks are lower efficiency and the industry's limited experience with lifetime performances.

Five different technologies are considered, one based monocrystalline, one on multicrystalline and three on thin films. The thin films will are exactly Copper, Indium, Selenide (CIS), Telluric, Cadmium (TeCd) and amorphous silicon.

The great majority of the commercial technologies belong to the five listed above.

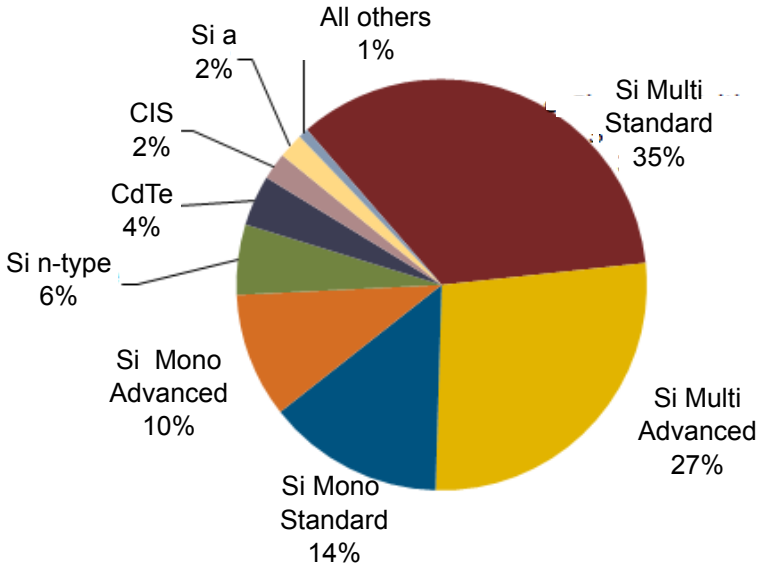

Figure 8.2: Solar PV Module Production by Technology on 2012, adapted from NPD Solarbuzz PV Equipment Quarterly report (www.solarbuzz.com/reports/pv-equipment-quarterly)

8.1 Efficiency

Depending on the technology, different value of the efficiency can be reached. Si- Mono modules are the most efficient. Multi-crystalline silicon modules have a slightly lower efficiency due to a lesser degree of order in

Technology	Efficiency (%)
Si Mono	16
Si Multy	15
CIS	11
TeCd	10
Si amorfo	6

Table 8.2: Table of the temperature's coefficient [33].

the atomic structure. However they are less expensive and more resistant to degradation due to irradiation

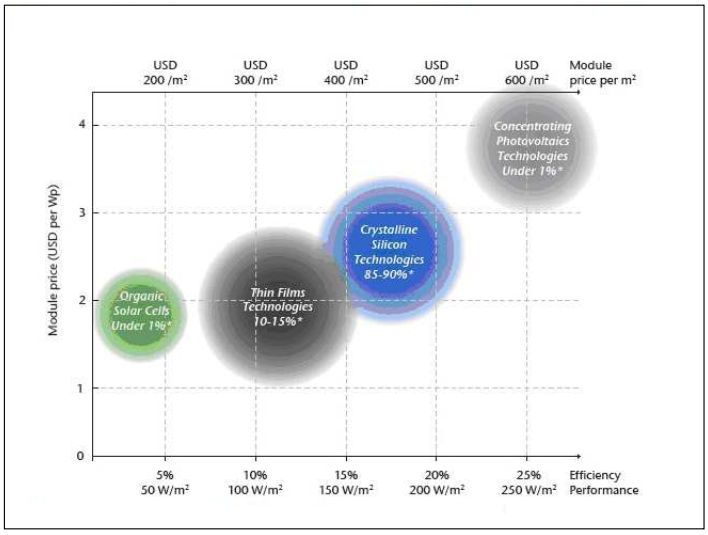

Figure 8.3: Performance and price range of different PV technologies (Source: International Energy Agency (IEA), technology roadmap-solar photovoltaic energy).

Modules with low efficiency like the thin films will require more roof than modules with higher efficiency in order to reach the same capacity. So, roof availability and cost must be taken into consideration when a technology is selected.

8.2 Installed power

Knowing the efficiency and the surface of the PV panels it is possible to estimate the power of the system using the equation [13]:

$$P = e\, A_{PV}\, G^* \tag{8.2}$$

with the irradiation $G^* = 1000kWh/m^2$. The maximum installed power is calculated assuming that all the suitable surface is covered by panels.

Fig.(8.4) shows the power that can be installed on each building that strongly depends on the technology adopted.

8.3 Performance ratio

Besides the efficiency it is necessary to take into account the performance ratio. The PR is relatively independent of the system power and of the location therefore is a basic parameter to compare different installation. In the PR are included all the type of losses that depends on the quality of the installation itself,

- electrical losses due shadow
- losses due to the temperature
- losses due to the tolerance of the power of the PV modules
- losses due to the dispersion of the parameters in the PV generator
- dirt losses
- angular and spectral losses
- losses due to the low irradiation
- losses in the DC wiring
- losses due to the tracking of the maximum power point of the inverter
- losses due to the inverter
- losses in the AC wiring

Usually the combination of all these losses give a perform ratio between 0.75 and 0.85 In this work are considered more carefully two losses: for temperature and for shadow.

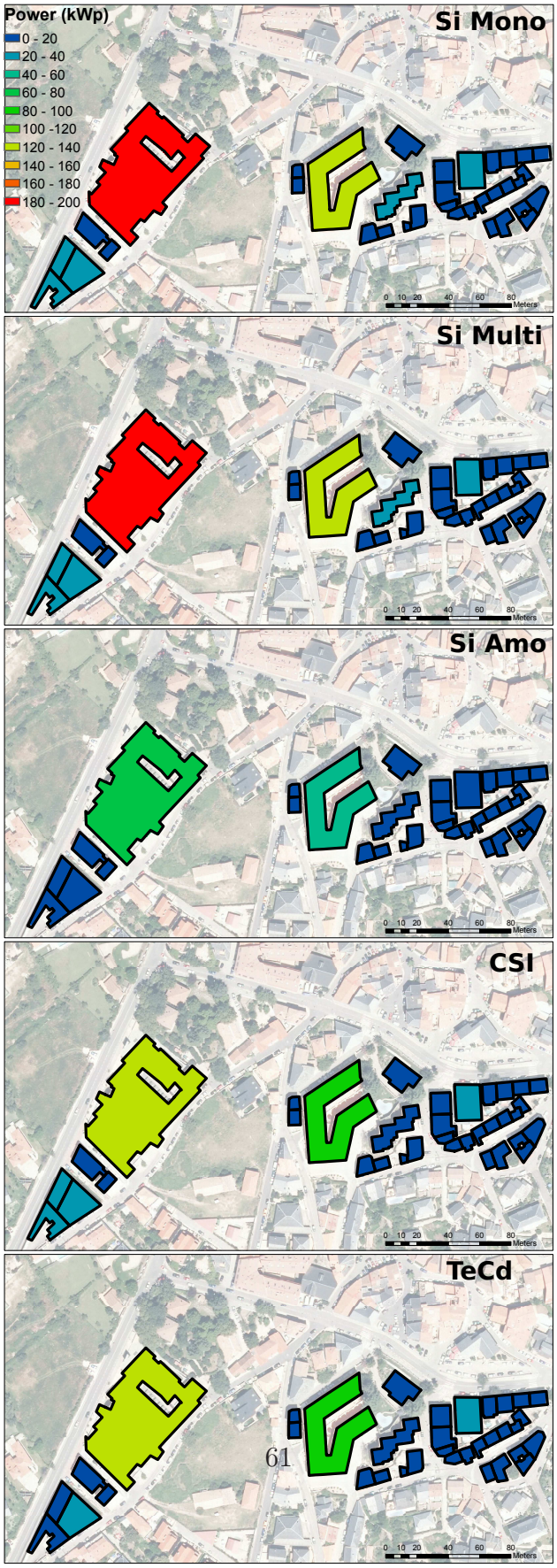

Figure 8.4: Installed power (kW_p) for the different technologies.

8.3.1 Shadow's effect

Calculate the losses due to the shadow are a really complicated task and an accurate description has to take into account the type of panel and the form of the shadow [34]. The real effect of partial shadings on the electrical production of the PV field is non-linear, and depends on the interconnections between the modules. In the PV array, the current of each cell string is limited by the current of the worst cell in the series. That is, when one only cell is shaded the entire string is strongly affected (which has also dramatic effects on the I/V characteristics of the whole array). This can be calculate with dedicated software as PVsyst. Such calculation is beyond the scope of this work. Instead, we want to estimate it in the most accurate way without knowing the details of the PV the type of the modules, the real string distribution of modules in space and the presence of by-pass protection diodes, (that plays an important role excluding the area that are effect by shadow so they do not lower the performance of the whole string). So only the geometry effects of the shadow taken into account. This means to assume that the reduction of the production of the electricity is just proportional to the fraction of the panels covered by the shadow. These losses are already taken into account in the irradiation model.

8.3.2 Temperature's effects

Another important factor in the operation of the PV panels is the temperature that can lead to relevant losses. The efficiency in Tab.(8.1) is given for an operation temperature of 25 degrees but usually the modules work a different temperature that most of the time is higher than 25 degrees. With higher temperature the efficiency decrees therefore, it is important to take into account this aspect. In order to calculate the real operation temperature it is necessary to know the conditions of the environment. In first approximation the operation temperature is given by:

$$T_o = T_e + G\frac{TNOC - 20}{800} \tag{8.3}$$

where T_e is the temperature of the environment, G is the irradiation on the PV panel and $TNOC$ is the temperature of the PV cell at the standard conditions, i.e. with $G = 800W/m^2$ and $T_e = 20^oC$. In this expression the effect of the wind that usually helps to refrigerate the PV panels is neglected. This effect can be considered with the more complex equation:

$$T_o = \frac{G}{G^*}\left(T_1 e^{bv} + T_2\right) + T_a + \frac{G}{G^*}\Delta T \tag{8.4}$$

Technology	Temperature's coefficient ($\%/^oC$)
Si Mono	0.43
Si Multy	0.43
CIS	0.38
TeCd	0.23
Si amorfo	0.21

Table 8.3: Table of the temperature's coefficient [33].

where the new parameters are: the STC radiance G^*, the temperature difference between the two face of the panel ΔT and the limit temperature for low/high wind's velocity $T_{1,2}$ and the cooling effect of the wind b. Once the real operation temperature is determinate, the equation

$$L_T = \gamma(T_o - T^*) \tag{8.5}$$

estimates the loss of the system due to the temperature. In the last equation T^* is the standard operation temperature, usually 25^o and γ is the temperature coefficient which is specified by the manufacturer. This strongly depends on the technology of the panel [Tab.(8.3)].

Eq.(8.5) can be easily implemented, calculate the hourly losses and sum them to have the annual loss but the difficulty comes from estimating the empirical parameters entering in Eq.(8.4). However, the uncertainty of these parameters makes pointless the use of such an accurate procedure. Therefore, it was decided to follow an alternative route.

The PVsyst allows to analyze the losses in percent of the annual production for panels of various technologies. In addition PVsyst has the advantage that allows us to simulate the different contributions of air cooling for free-standing panels and for panels overlaid on the roof. The two different typologies can reach difference on the temperature of the order of $10^o - 20^oC$ thanks to the cooling of the wind. In this way a fairly realistic estimation of the losses depending on the technology and on the mounting mode of the modules can be obtained.

The basic equation is the energy balance between ambient temperature and cell's heating up due to incident irradiation:

$$U(T_o - T_{amb}) = \alpha\, G(1 - Ef) \tag{8.6}$$

where U is the thermal loss factor which can be split into a constant component U_c and U_v a factor proportional to the wind velocity v :

$$U = U_c + U_v v. \tag{8.7}$$

Technology	Overlaid (%)	Free standing (%)
Si Mono	6	4
Si Multy	6	4
CIS	5.5	3
TeCd	5.2	2.8
Si amorfo	3.6	2

Table 8.4: Losses for temperature.

Ef is the energy removed from the module and α is the absorption coefficient of solar irradiation. The default value are $Ef = 10\%$ and $\alpha = 0.9$ and

$$U_c = 29W/m^2k\,, \qquad U_v = 0W/m^2k/m/s \tag{8.8}$$

for free-standing panels that in our study correspond to the panels mounted on "flat" roof, according with the definition in Ch.(5), and

$$U_c = 20W/m^2k\,, \qquad U_v = 0W/m^2k/m/s \tag{8.9}$$

for overlaid panels namely, panels on sloping roof. The result of this analysis conduct using PVsyst is in Tab.(8.4)

8.3.3 Losses

Moreover there are the losses due to the dispersion of the parameters in the PV generator. Normally the real parameters of the PV modules have an uncertainty that is specified by the manufacturer. This implies losses that can be estimated as 2%[32]. Another cause of system losses is the dirt that can accumulate on the modules. The dirt can be of two types: uniform, like dust, air pollution or localized, perhaps the effect beach (accumulation of sand near to the frame) or bird droppings. In the first case there is decrease of captured radiation and in the second one there is an increase of the dispersion of parameters and generation of hot spots with resulting losses. The main factors which determine the dirt of the modules are: air pollution, bird droppings, rainfall, slope of modules, and proximity to the ground, cleaning of modules (intervals and efficiency). In this work the factor of loss for dirt is equal to 3% [32]. As seen previously a temperature of operation different from the STC provoke losses, the same applies to other factors. An irradiation lower then $1000W/m^2$ causes losses for low irradiation, an angle of incidence other than 90 degrees leads to angular losses and an

Technology	Overlaid (%)	Structure (%)
Si Mono	26	24
Si Multy	26	24
CIS	25.5	23
TeCd	25.2	22.8
Si amorfo	23.6	22

Table 8.5: Loses.

absolute air mass different from 1.5 origin spectral losses. In total these losses are around the 6% [32], [35]. The losses in the dc part of the wiring dc part of the wiring due to an overheating of the cables correspond to 1% [32].

Still are missing the losses due to the inverter that depend on the instant value of the current. For one accurate determination of the annual loss should be calculate the hourly loss and sum over the whole year. But it is enough estimate an annual percentage of loss, following what done for the temperature losses. Those losses are in the range of $4 - 9\%$ according with [10] and PVSyst. At the end the loss due to the AC wiring are 1% [32].

Finally, Tab.8.5 summarizes the estimation, used in this work, of the total losses [32, 10][1].

With this approach the hourly performance ratio is approximated with an annual factor therefore, the Eq.(8.1) becomes

$$E_{annual} = A_{PV} PR\, e \sum_h I_g^h \tag{8.10}$$

This is used to estimate the annual energy production.

8.4 Results

In Fig.(8.5) the annual energy production pro square is represented. The production varies depending on the amount of irradiation received by the panels and the technology adopted. This map helps to recognize the best places to locate PV systems. The most productive parts are the flat roofs where the panels can be arranged at the optimum and the roofs that are

[1]PVSyst is used to perform some simulations and calculate the PR of a simple PV system with only a single panel disposed at the optimum, this is not a general valid answer for the problem of the losses but only a first estimation.

oriented to the south and with an inclination around 32 degrees and without shadow.

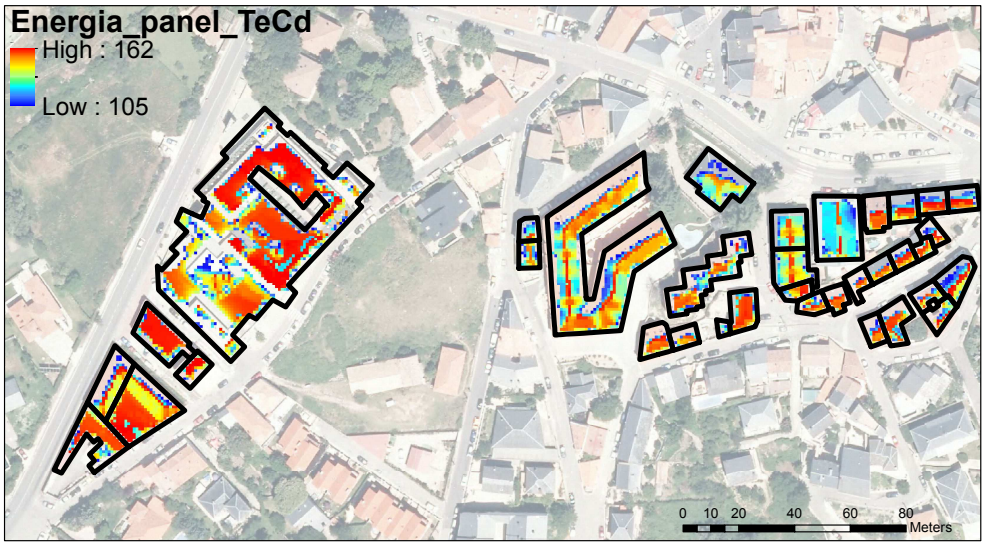

Figure 8.5: Annual energy production pro square meter using panels of TeCd

Fig.(8.6) shows the annual production of each buildings, clearly this depends on the suitable surface and on the technologies adopted. Using a technology with higher efficiency like Si-Mono or Multi the production is substantially higher. The comparison between the different technologies can help to decide which is the more appropriate technology depending on the desired amount of energy production.

One important factor to choose the most attractive buildings to install PV systems is the number of equivalent hours. This number allows comparing the quality of an installation. Fig.(8.7) shows the number of equivalent hours for each building using panel of TeCd (for the other technologies the results are similar and are reported in App.F). Except for two small buildings on the right, the more suitable roofs for a PV system are the three on the left which have a part of the flat roof. In particular the petrol station with a flat roof without shadow where it is possible to install a system with a high efficiency.

To better compare the different results in Tab.(8.6) it is summarized the total annual energy production, the total installed power of the entire area of study and the equivalent hours for each technologies. The installed power and the energy vary. The production is of $324 MWh$ in front of a installed

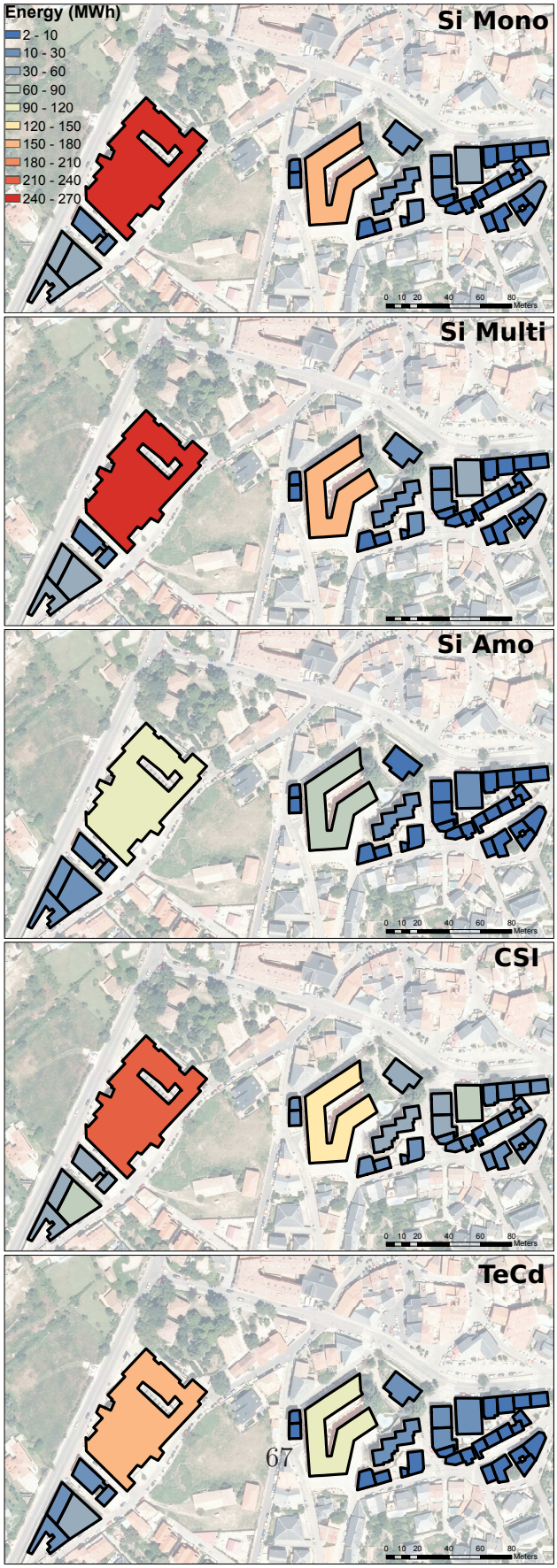

Figure 8.6: Annual energy production (kWh) of each building using different technologies.

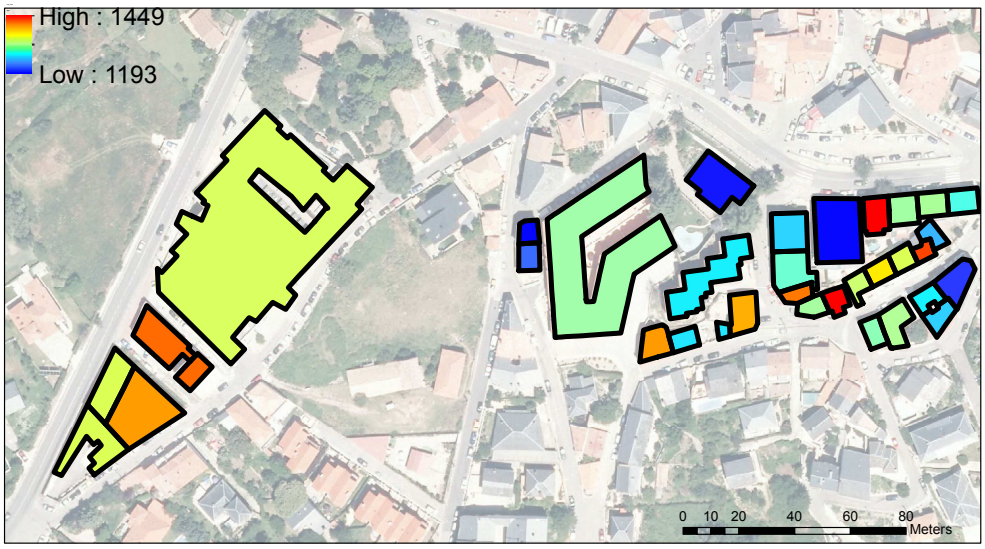

Figure 8.7: Number of equivalent hours of PV sysem using TeCd panels

Technology	Power (kW_p)	Energy (MWh)	Hours
Si Mono	622	814	1308
Si Multy	589	764	1310
CIS	427	564	1319
TeCd	408	540	1324
Si amorphous	235	312	1338

Table 8.6: Loses.

power of $241kWh_p$ using panels of Si amorphous and reaches $846MWh$ with a installed power of $641kWp$ in the case of Si monocrystalline. Using a more efficent technology it is possible to obtain a increase of 160% in the production. The panels of Si multicrystalline have similar efficiency to the ones of Si multicrystalline therefore the production comparable. The othere two technologies (CIS and TeCd) offere a intermediate production. Instead the number of equivalent hours is similar in all case. The small difference is due to the different losses due to the temperature. For example, panels of Si-Amorphous that have better performance a high temperature have as well a slightly higher number of equivalent hours although the difference is note relevant. This kind of comparison becomes more important studying area with higher temperature.

Fig.(8.8) shows the last result, the occupancy factor of the roof which is defined as the ratio between the surface of the roof and surface usable to mount PV panels. Smaller values are obtained for buildings with roof

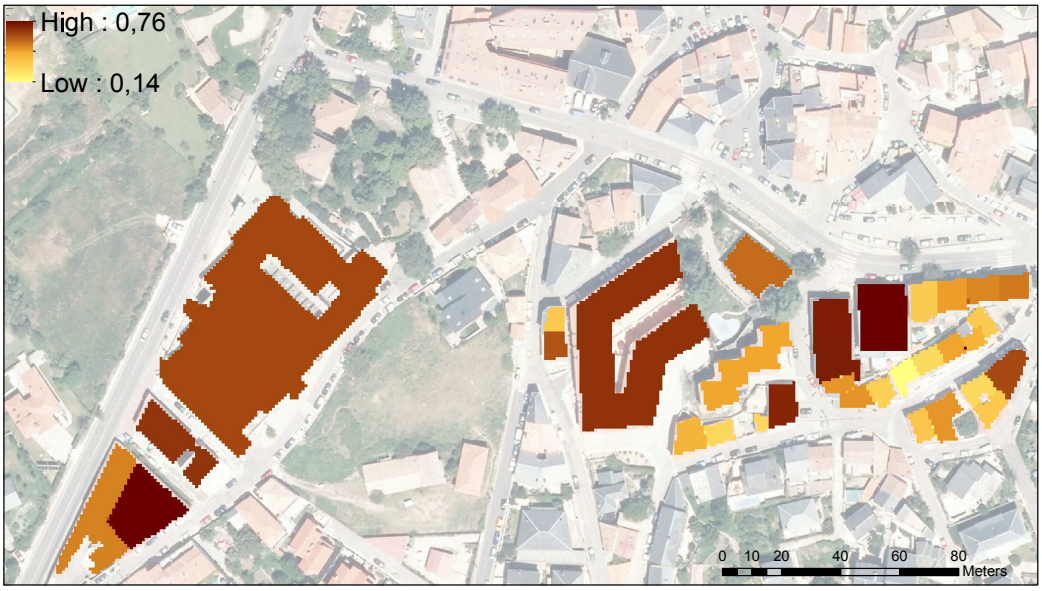

Figure 8.8: Occupation factor

oriented north-south, where the north part of the roof can not be used. The presence of trees or buildings higher than the roof itself makes as well the occupancy factor lower due to the presence of shadows. Instead buildings with flat roof and oriented east west tend to have a higher occupancy factor. In total the occupancy factor in the area is 54%.

Conclusion

The implementation of PV in urban areas requires careful Multi-criteria analysis of a large number of variables associated with spatial entities, and without any doubt GIS respond adequately to the needs of this type of study. This work presents a pilot study on a small area of the municipality of Miraflores de la Sierra, which is based on data LIDAR has allowed to develop a model and know the potential in photovoltaic applications in urban areas. First the LIDAR data are manipulated with the software "VRMash Stuidio" and second the result is imported in an ARCGIS model and the MDS of the entire are of study is obtained, containing all the elements (buildings, streets, trees...). This is used to create a map of the shadow and as well to identify the areas those are suitable to place a PV system. To do this it is necessary to identify the surface of the roofs using the "catastro". Two filter are applied, one to discriminate the monuments and landmarks buildings and a second one to exclude a perimetric area of the roofs that has to be let free. For the remaining area the local inclination and orientation are calculated. With this information two typologies of roofs are differentiated. The first one where the PV panels are placed parallel to the roof and the second one where the panels are disposed at the optimum using structure. For the first typology the irradiation incident the roof simply is calculated using the shadow's map and the map of the inclination and orientation of the roofs. For the second type the proceed is similar but since the panels are not parallel to the roof it is necessary to introduce a correction factor. In this way it is possible to obtain a map of the solar potential I_g. It is not possible to exploit all this energy. The local irradiation depends from the inclination and orientation of the roof and the presence of elements that cast a shadow therefore, on a portion of the roofs the annual irradiation is too low and it is not economically viable to install PV panels, so two threshold depending of the type of the roof discriminate where the annual irradiation is enough to make viable the installation of a PV system. Once that, the amount of the irradiation that can be used to generate current is known the effective

production is evaluated taking into account the efficiency of the panels and difference sources of losses. The operation temperature is an important factor of loss and it strongly depends on the technology adopted and type of installation. The losses of five different technologies go from only 2% for a panel of Si amorphous mounted on a free standing structure to the 6% for a panel of Si monocrystalline overlaid to the roof. Our model allowing to compare the performance of different technologies, simplifies the choice of the most suitable technology. In the future it will be useful to include in the model a section devoted to the consumption of individual buildings, allowing a comparison with the production of the buildings.

A important result is the estimation of the suitable surface. Using a more accurate method leads to a more optimistic result respect to the one of the preceded work [13]. As well the possibility to optimize the disposition of the panels on flat roof leads an increase of the annual production. Therefore can be interesting add to the model a more complex way to optimize the surface of the roof, without being restricted to the "flat" or "sloping" typologies. The creation of a 3D map of the city center as accurate as possible is in our opinion, essential for the development of this toolbox This can be done improving the resolution of the LIDAR data and developing new algorithms that can detect with precision the form of buildings and elements above them.

Appendix A

Environment's shadow

The "Hillshade" tool determines the illumination of an area from raster surface model taking into account the position of the sun. This toolbox provides one raster for each hour where 0 means that not shadow is present and 1 indicate the presence of shadow. The picture (A)-(A.2) shows the evolution of the shadow during two typical day of the year

Figure A.1: Shadow calculate with the toolbox "Hillshade" for the day of the winter solstice at two-hour intervals starting from 8 a.m (top right) up to 14 p.m. (latest below)

Figure A.2: Shadow calculate with the toolbox "Hillshade" for the day of the summer solstice at two-hour intervals starting from 6 a.m (top right) up to 18 p.m. (latest below)

Appendix B

Solar map's algorithm

As first thing the different inclinations and orientations are divide in 5 in 5 degrees .

β	m
$0-5$	1
$5-10$	2
$10-15$	3
$15-20$	4
...	...
$75-80$	18
$80-85$	19

(B.1)

α	n
$-180- -175$	1
$-175- -170$	2
...	...
$170-175$	71
$175-180$	72

(B.2)

Then an unique index z is created for the various combinations of inclination and orientations.

$$z = n * 100 + m \tag{B.3}$$

that goes from 11 to 7300

In order to include the shadow in a unique index, negative value are introduced (from -7300 to -11), as well. Where negative value are associated

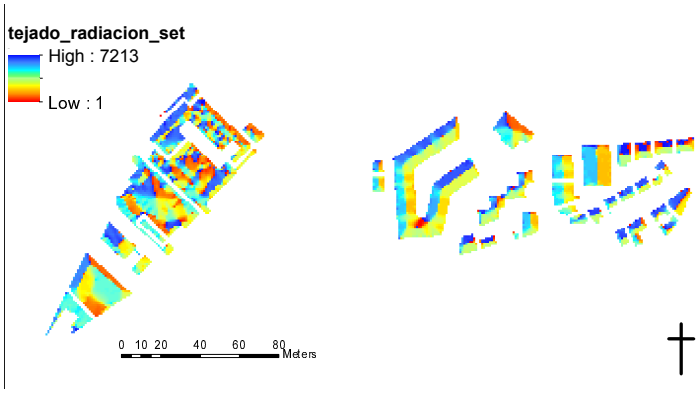

Figure B.1: Maps of the z parameter.

with shadow and positive ones without. The model in FigB.2 calculates the z index where first the inclination and orientation raster are catalogued following the tables (B.2) and (B.1) then we use a "Raster calculator" toolbox to calculate the z index as in Eq.(B.3) and finally multiply this z-Index Raster with the Raster of the shadow the finally raster is obtained. This last operation as to be performed for each hour of the year. The shadow of the PV panel itself is take into account on a later step. In this way a single raster contains all the information about the panels necessary to calculate the amount of solar radiation that they receive.

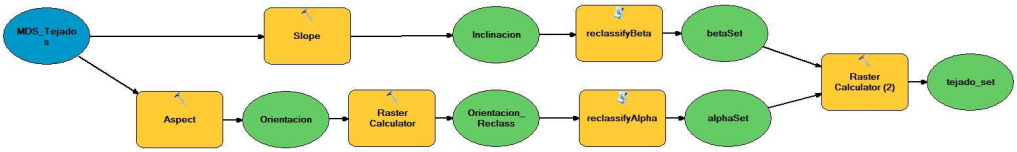

Figure B.2: Model set

After this for every hour, the "radiation table" toolbox creates a table with the solar radiation relative at the index z and this is used the reclassify the z index raster and associates at each point of the roof raster his "available radiation". The result is not strictly speaking the radiation incident each point of the roof because the correction factor introduced in Chapter 5 has been already taken into account.

Appendix C

PVgis

The PVgis web page offers the possibility to estimate the annual electricity production from the given system including losses due to temperature low irradiance reflectance effects, cables, inverter and other minor losses. It gives

Technology	Buildings Integrated (%)	Free standing (%)
Si Mono	13	8
CIS	11	7
TeCd	4.2	1.3

Table C.1: Estimated losses due to temperature and low irradiance by PVgis using local ambient temperature.

as well an estimation of the losses due to temperature and low irradiance, there is a small difference with the results obtained with PVsyst. It can be due to the usage of slightly different temperature's coefficients.

Appendix D

Hourly production

Fig.(D.1) shows the variation during typical day of spring without claud of the energy production.

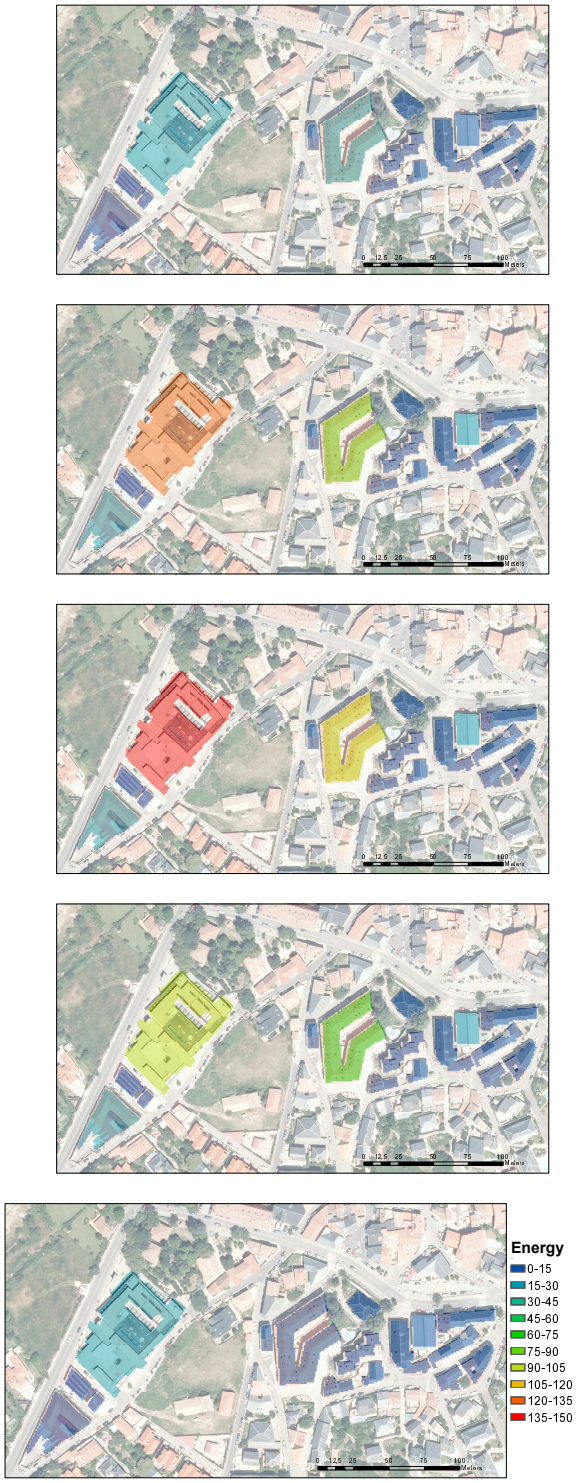

Figure D.1: Hourly energy production of each building using TeCd. Starting from the top left figure at 6 am, 9am, 12am, 15 am and 18 am

Appendix E

Model

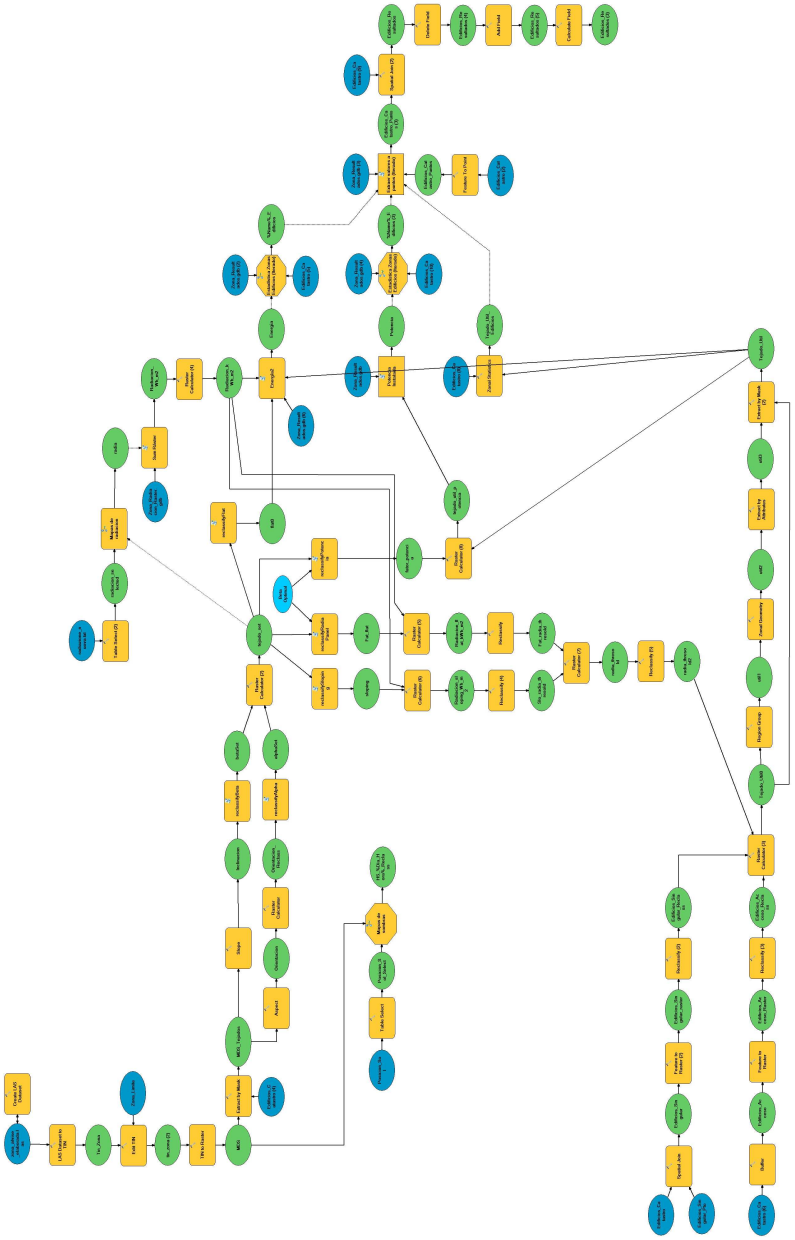

Figure E.1: Model

Appendix F

Buildings Results

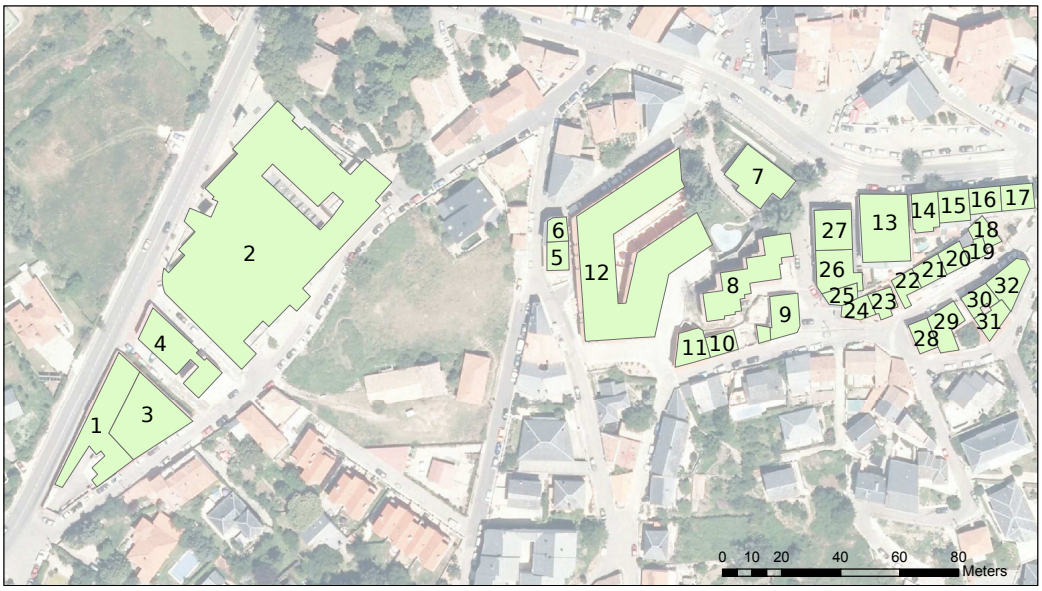

Figure F.1: Buildings numeration.

Building	Surface	Si Mono	Si Multi	CIS	TeCd	Si Amorfo
1	222	29,7	27,8	20,4	19,5	11,1
2	1759	200,6	188,1	137,9	131,7	75,2
3	317	39,0	36,5	26,8	25,6	14,6
4	182	19,3	18,1	13,3	12,7	7,3
5	39	5,8	5,5	4,0	3,8	2,2
6	19	2,9	2,7	2,0	1,9	1,1
7	136	20,2	19,0	13,9	13,3	7,6
8	146	22,8	21,4	15,7	15,0	8,5
9	81	10,4	9,8	7,2	6,8	3,9
10	43	6,4	6,0	4,4	4,2	2,4
11	242	37,4	35,1	25,7	24,6	14,0
12	38	5,7	5,3	3,9	3,7	2,1
13	49	7,1	6,6	4,9	4,6	2,7
14	44	6,1	5,7	4,2	4,0	2,3
15	46	6,6	6,2	4,5	4,3	2,5
16	20	2,8	2,6	1,9	1,8	1,1
17	17	2,2	2,1	1,5	1,5	0,8
18	30	4,1	3,8	2,8	2,7	1,5
19	22	3,1	2,9	2,2	2,1	1,2
20	14	1,9	1,8	1,3	1,3	0,7
21	22	3,2	3,0	2,2	2,1	1,2
22	30	4,4	4,1	3,0	2,9	1,6
23	26	3,6	3,4	2,5	2,4	1,4
24	112	17,2	16,2	11,9	11,3	6,5
25	107	16,3	15,3	11,2	10,7	6,1
26	25	3,7	3,4	2,5	2,4	1,4
27	75	10,9	10,2	7,5	7,2	4,1
28	57	7,5	7,1	5,2	5,0	2,8
29	28	4,1	3,9	2,8	2,7	1,5
30	23	3,4	3,2	2,4	2,2	1,3
31	27	4,0	3,7	2,7	2,6	1,5
32	860	131,4	123,2	90,3	86,2	49,3
Tot	4858	644,1	603,8	442,8	422,7	241,5

Figure F.2: Installed power (kW_p) on each building and for the five different technologies.

Building	Surface	E Si Mono	E Si Multi	E CIS	E TeCd	E Si Amorfo
1	222	39687	37207	27542	26376	15140
2	1759	267489	250771	185705	177831	101830
3	317	54069	50690	37520	35933	20632
4	182	27121	25426	18841	18040	10291
5	39	7219	6768	5001	4791	2778
6	19	3449	3233	2389	2289	1326
7	136	24523	22990	16990	16277	9432
8	146	29165	27342	20190	19347	11261
9	81	14380	13481	9985	9561	5469
10	43	8946	8387	6196	5937	3446
11	242	44228	41463	30618	29338	17078
12	38	8128	7620	5630	5394	3132
13	49	9292	8711	6440	6169	3568
14	44	7982	7483	5535	5302	3056
15	46	8472	7943	5872	5625	3251
16	20	3542	3321	2456	2352	1357
17	17	3161	2963	2195	2102	1203
18	30	5463	5122	3789	3629	2092
19	22	4282	4015	2968	2843	1644
20	14	2589	2428	1795	1720	993
21	22	4522	4240	3133	3002	1739
22	30	5781	5420	4005	3837	2224
23	26	5091	4772	3531	3382	1947
24	112	22357	20959	15481	14833	8621
25	107	20748	19451	14368	13767	7998
26	25	4804	4504	3328	3188	1850
27	75	13314	12482	9227	8840	5113
28	57	9927	9307	6887	6596	3792
29	28	5258	4929	3642	3489	2024
30	23	4382	4108	3035	2907	1688
31	27	5047	4732	3497	3350	1941
32	860	172333	161562	119331	114338	66464
Tot	4858	846750	793828	587123	562385	324377

Figure F.3: Energy produced (kWh) on each bulding and for the five different technologies.

Building	Surface	Si Mono	Si Multi	CIS	TeCd	Si Amorfo
1	222	1337	1337	1349	1354	1360
2	1759	1333	1333	1346	1351	1353
3	317	1387	1387	1400	1405	1412
4	182	1402	1402	1417	1421	1419
5	39	1238	1238	1248	1253	1271
6	19	1209	1209	1219	1223	1240
7	136	1212	1212	1221	1226	1243
8	146	1280	1280	1289	1293	1318
9	81	1381	1381	1395	1399	1401
10	43	1390	1390	1400	1406	1428
11	242	1181	1181	1189	1194	1216
12	38	1433	1433	1444	1449	1473
13	49	1311	1311	1322	1327	1343
14	44	1314	1314	1326	1330	1342
15	46	1289	1289	1300	1304	1319
16	20	1260	1260	1270	1275	1287
17	17	1415	1415	1429	1434	1436
18	30	1337	1337	1348	1353	1365
19	22	1364	1364	1375	1380	1396
20	14	1329	1329	1340	1345	1359
21	22	1429	1429	1441	1446	1466
22	30	1314	1314	1324	1329	1348
23	26	1399	1399	1412	1416	1427
24	112	1297	1297	1306	1311	1333
25	107	1271	1271	1280	1285	1306
26	25	1306	1306	1316	1320	1341
27	75	1221	1221	1231	1236	1251
28	57	1316	1316	1328	1332	1340
29	28	1275	1275	1285	1290	1309
30	23	1280	1280	1289	1294	1315
31	27	1269	1269	1279	1284	1302
32	860	1312	1312	1321	1326	1349
Tot	4858	1315	1315	1326	1331	1343

Figure F.4: Number of equivalent hours on each bulding and for the five different technologies.

Bibliography

[1] A. G. Hestne. Building integration of solar energy systems. *Solar Energy*, 67:181 – 187, 1999.

[2] M. La Gennusa et. al. A model for predicting the potential diffusion of solar energy systems in complex urban environments. *Energy Policy*, 39:5335 – 5343, 2011.

[3] H. T. Nguyen and J. M. Pearce. Incorporating shading losses in solar photovoltaic potential assessment at the municipal scale. *Solar Energy*, 90:730–741, 2012.

[4] J. Giesekam J. Gooding, H. Edwards and R. Crook. Solar city indicator: A methodology to predict city level pv installed capacity by combining physical capacity and socio-economic factors. *Solar Energy*, 95:325–335, 2013.

[5] J. A. Voogt T. R. Tooke, N. C. Coops and M. J. Meitner. Tree structure influences on rooftop-received solar radiation. *Landscape and Urban Planning*, 102:73–81, 2011.

[6] M. Rodrigues S. Izquierdo and N. Fueyo. A method for estimating the geographical distribution of the available roof surface area for largeÂ-scale photovoltaic energyÂpotential evaluations. *Solar Energy*, 82:929–939, 2008.

[7] Mainzer K. et al. A high-resolution determination of the technical potential for residential-roof-mounted photovoltaic systems in germany. *Solar Energy*, 105:715–731, 2014.

[8] J. Giesekam J. Gooding, H. Edwards and R.Crook. Solar city indicator: A methodology to predict city level pv installed capacity by combining physical capacity and socio-economic factors. *Solar Energy*, 95:325–335, 2013.

[9] M. Pomerant R. Levinson, H. Akbari and S. Gupt. Solar access of residential rooftops in four california cities. *Solar Energ*, 83:2120–2135, 2009.

[10] B.Marion and al. Performance paramters for grid-connected pv systems. In *31st IEEE Photovoltaics Specialists*, 2008.

[11] Boyson W.E. Cameron, C.P. and Riley D.M. Comparison of pv system performance-model predictions with measured pv system performance. In *Photovoltaic Specialists Conference, San Diego*, 2008.

[12] P. Fu and P.M. Rich. Design and implementation of the solar analyst: an arcview extension for modeling solar radiation at landscape scales. In *Proceedings of the Nineteenth Annual ESRI User Conference*, 1999.

[13] A. M. Martin Avila. Modelo geografico para la estimacion del potencial fotovoltaico en tejados. caso de estudio:miraflores de la sierra. Master's thesis, Universitad Complutense de Madrid, 2013.

[14] M. Suri and J. Hofierka. A new gis-based solar radiation model and its application to photovoltaic assessments. *Transactions in GIS*, 8:175 – 190, 2004.

[15] T. Santos M.C. Brito, N. Gomes and J.A. Tenedorio. Photovoltaic potential in a lisbon suburb using lidar data. *Solar energy*, 86:283–288, 2012.

[16] J. A. Jakubiec qnd C. F. Reinhart. A method for predicting city-wide electricity gains from photovoltaic panels based on lidar and gis data combined with hourly daysim simulations. *Solar Energy*, 93:127 – 143, 2013.

[17] N. Gomes. Master's thesis, MSc Thesis, New University of Lisbon, 2011.

[18] B. L. Bhaduri J. B. Kodysh, O. A. Omitaomu and B. S. Neish. Methodology for estimating solar potential on multiple building rooftops for photovoltaic systems. *Sustainable Cities and Society*, 8:31–41, 2013.

[19] N. Lukac et al. Rating of roofs surfaces regarding their solar potential and suitability for pv systems, based on lidar data. *Applied Energy*, 102:803–812, 2013.

[20] T. Chaves and A. T. Bahill. Locating sites for photovoltaic solar panels. pilot study uses dem derived from lidar. *ESRI*, 2010.

[21] H. T. Nguyen. The aplication of lidar to assessment of rooftop solar photovoltaic deployment potential in municipal district unit. *Sensors*, 12:4534 – 4558, 2012.

[22] J.E. Hay. Calculation of monthly mean solar radiation for horizontal and inclined surfaces. *Solar Energy*, 23:301 – 307, 1979.

[23] E. Lorenzo. *Electiricidad Solar, Vol. II.* Progensa, 1994.

[24] Poggi P. Louche A., Notton G. and Simonnot G. Correlations for direct normal and global horizontal irradiation on a french mediterranean site. *Solar Energy*, 45:9–17, 1991.

[25] Beckman W. A. Reindl D. T. and Duffie J. A. Evaluation of hourly tilted surface radiation models. *Solar Energy*, 46:261–266, 1990.

[26] L. Zarzalejo et al. A new statistical approach for deriving global solar radiation from satellite images. *Solar Energy*, 83:480–484, 2009.

[27] M. Lefevre C. Rigollier and L. Wald. The method heliosat-2 for deriving shortwave solar radiation from satellite images. *Solar Energy*, 77:159–169, 2004.

[28] Zarzalejo et al. J. Polo. Estimation of daily linke turbidity factor by using global irradiance measurements at solar noon. *Solar Energy*, 83:1177–1185, 2009.

[29] M. A. Egido. Radiación solar. In *Máster en Energías Renobles y Medio Ambiente, Universidad Politecnica Madrid*, 2013/2014.

[30] E. Lorenzo. *Electiricidad Solar, Vol. III.* Progensa, 2013.

[31] IDAE. Instalaciones de energía solar fotovoltaica. In *Pliego condiciones técnicas ins talaciones conectadas a red*, 2011.

[32] J. Amador. Presentacion: analisis energeticos sfvcr. In *Máster en Ingeniería de la Energía, Universidad Politecnica Madrid*, 2014.

[33] N. Martin Chivelet. *Integracion de la enrgia fotovoltaica en edificios.* progensa, 2011.

[34] C. Delinea et al. A simplified model of uniform shading in large photovoltaic arrays. *Solar Energy*, 97:274 – 282, 2013.

[35] Martín N. and Ruiz J.M. *Solar Energy Material Cells*, 70, 2001.

Online Resouces

[1] PVWatts
www.nrel.gov/rredc/pvwatts/

[2] PVGIS
re.jrc.ec.europa.eu/pvgis/apps4/pvest.phpadra

[3] Adrase
www.adrase.es

[4] Agencia estatal de meterología
www.aemet.es/es/serviciosclimaticos/datosclimatologicos

[5] Urban Atlas
www.eea.europa.eu/data-and-maps/data/urban-atlas

[6] Infraestructura de Datos Espaciales Comunidad de Madrid
www.madrid.org/cartografia/idem

1135-9420